Journal of Structural Geology 32 (2010) 941–959

Contents lists available at ScienceDirect

Journal of Structural Geology

journal homepage: www.elsevier.com/locate/jsg

Tectonic implications for a Cordilleran orogenic base in the Frenchman Cap dome, southeastern Canadian Cordillera

Félix Gervais [a,*], Richard L. Brown [a], James L. Crowley [b]

[a] Department of Earth Sciences, Carleton University, Ottawa, ON, Canada K1S 5B6
[b] Department of Geosciences, Boise State University, Boise, ID 83725, USA

ARTICLE INFO

Article history:
Received 26 December 2009
Received in revised form
6 May 2010
Accepted 13 May 2010
Available online 20 May 2010

Keywords:
Gneiss dome
U–Pb geochronology
Strain gradient
Frenchman Cap dome
Southern Canadian Cordillera

ABSTRACT

The Frenchman Cap gneiss dome of the Monashee Complex in the Canadian Cordillera sits in basement rocks of the orogen. It records a stepwise downward disappearance of penetrative deformation indicative of a frozen downward-migrating base of easterly verging Cordilleran shearing. This tectonic setting is incompatible with the commonly held views that gneiss domes of the Canadian Cordillera are extensional core complexes and that the presence of gneiss domes in orogens implies vertical flow. An important structural-time marker in our study is a widely distributed suite of ~1850 Ma granite dykes that allow Cordilleran-aged structures to be distinguished from the older structures. The dykes show that only the uppermost ~1.5 km structurally thick carapace of basement gneiss records penetrative Cordilleran strain, whereas the lowermost ~5 km thick basement section does not and instead preserves a Paleoproterozoic migmatitic gneissosity. Cordilleran high strain in the upper basement carapace is characterized by penetrative easterly verging shear strain on both the westerly dipping and easterly dipping flanks of the dome, whereas Cordilleran deformation in the lower basement is limited to a meter-scale, top-to-the-east shear zone and NNE-trending, upright folds. New and previously published U–Pb data from accessory minerals indicates that the Cordilleran structures formed between 53 and 49 Ma, immediately prior to regional cooling and extension. The dome is interpreted as an incipient upright drag fold developed during top-to-the-east shearing.

1. Introduction

Gneiss domes are common structures of orogens that offer a window into deep crustal processes. In a review of gneiss domes, Whitney et al. (2004) argued that they are a manifestation of crustal flow, irrespective of the mechanism that led to their formation (e.g., folding, rolling-hinge, diapirism). Several gneiss domes are exposed in the southeastern Canadian Cordillera, notably the Frenchman Cap and the Thor-Odin domes of the Monashee Complex, and the China, Passmore, and Valhalla domes of the Valhalla Complex. The origin of these domes has generally been related to extension (Carr et al., 1987; Parrish et al., 1988; Vanderhaeghe et al., 1999; Kruse and Williams, 2007), and the Thor-Odin dome was presented as a type-case of a dome formed by vertical ductile flow of partially molten middle crust during the gravitational collapse of a thickened orogen (Teyssier and Whitney, 2002; Whitney et al., 2004; Teyssier et al., 2005). However, studies of the adjacent Frenchman Cap dome point to a drastically different history. Crowley et al. (2001) documented a downward-decreasing strain gradient in the dome based on the deformation state of Paleoproterozoic granite and pegmatite dykes (Crowley et al., 2008). These data led to models of progressive downward migration of the base of convergent ductile shearing with time (Parrish, 1995; Gibson et al., 1999; Crowley et al., 2001; Brown, 2004). Inasmuch as studies from the Thor-Odin dome were pivotal to deriving a paradigm of gneiss dome formation and orogenic collapse (Vanderhaeghe and Teyssier, 2001; Teyssier and Whitney, 2002; Whitney et al., 2004; Teyssier et al., 2005), it is crucial to assess the validity of the contradictory conclusions derived from the Frenchman Cap dome.

The first aim of this study is to determine whether the granite dykes dated by Crowley et al. (2001, 2008) could be used as time markers to determine the age of deformation throughout the basement of the Frenchman Cap dome of the Monashee Complex. The second aim is to better characterize the strain gradient reported by Crowley et al. (2001) and assess the nature and age of deformation from other parts of the dome, including those at the deepest structural level. Finally, a tectonic model for the dome is proposed.

* Corresponding author. Present address: Department of Earth & Planetary Sciences, McGill University, Adams Building, 3450 University Street, Montreal, QC, Canada H3A 2A7. Tel.: +1 514 398 5884.
E-mail address: felix.gervais@mcgil.ca (F. Gervais).

0191-8141/$ – see front matter © 2010 Elsevier Ltd. All rights reserved.
doi:10.1016/j.jsg.2010.05.006

2. Geological setting

The Monashee Complex occupies the deepest structural level of the Omineca Belt that forms, along with parts of the Coast Plutonic Belt, the core zone of the Canadian Cordillera (Fig. 1). The belt is east of the Insular, Coast Plutonic and Intermontane belts, which consist of pericratonic and exotic terranes accreted to the western margin of the North American craton in the Jurassic to Early Cretaceous (Evenchick et al., 2007). To the east lies the Foreland Belt, which records 200 km of shortening between 75 and 59 Ma (Price and Sears, 2000). The Canadian Cordillera was thus under compression from the Jurassic to the Paleogene. The end of orogeny in the southern Omineca Belt is marked by 1) 53–48 Ma $^{40}Ar/^{39}Ar$ mica cooling ages recorded throughout (Scammell, 1993; Bardoux, 1994; Johnson, 1994; Sanborn, 1996; Vanderhaeghe et al., 2003; Ghent and Villeneuve, 2006); 2) the 51–47 Ma bracket for the last increments of ductile shearing along two outward-dipping normal brittle–ductile shear zones that bound the belt (Glombick et al., 2006; Mulch et al., 2006); and 3) the ~48 Ma emplacement age of undeformed lamprophyre dykes with chilled margins (Adams et al., 2005). The 53–47 Ma period was thus one of regional cooling accompanied with extension.

The Monashee Complex consists of two gneiss domes: Frenchman Cap dome (FCD) in the north and Thor-Odin dome (TOD) in the south (Fig. 1). It is fault-bounded, with a westerly dipping, top-to-the-east ductile shear zone termed the Monashee décollement, on its west flank; and an easterly dipping, top-to-the-east brittle–ductile shear zone, termed the Columbia River fault, on its east flank (Figs. 1 and 2). The complex is flanked by the sillimanite-K-feldspar grade rocks of the Lower Selrkirk allochthon in the hanging wall of the Monashee décollement, and the garnet grade rocks of the Upper Selkirk allochthon in the hanging wall of the Columbia River fault (see Gervais, 2009 for more details about these terms). The domes are cored by Paleoproterozoic gneiss, termed basement, and mantled by metasedimentary rocks, termed cover sequence, that are inferred as having been deposited on the passive margin of North America in the Precambrian (Scammell and Brown, 1990; Crowley, 1999). The base of the cover sequence consists of a quartzite layer that delineates the shape of the domes, and thus constitutes an important structural marker (Fig. 1). The cover sequence is infolded with pervasively deformed basement slices, whereas basement rocks prevail below the basal quartzite (Fig. 1).

2.1. Summary of deformation in the core of the Thor-Odin dome

Several studies investigated structurally deep levels of the TOD. The Blanket Mountain area (C in Fig. 1), located at the contact between the basal quartzite and basement paragneisses, records top-to-the-NE deformation and amphibolite facies metamorphism between 57 and 51 Ma (Johnston et al., 2000). The Saturday Glacier area (D in Fig. 1), located ~1.5 km structurally below the basal quartzite, consists mainly of migmatitic paragneisses that record partial melting, decompression and top-to-the-northeast shearing between 56 and 52 Ma (Hinchey et al., 2006). The Bearpaw Lake area (E in Fig. 1), located ~1 km structurally below the basal quartzite, was key to deriving models of crustal flow and diapirism (Vanderhaeghe et al., 1999; Teyssier and Whitney, 2002; Teyssier et al., 2005) because a metatexite–diatexite transition indicating a dome-up sense of shear was mapped (Vanderhaeghe et al., 1999) and an isothermal decompression path was documented for migmatitic schists (Norlander et al., 2002). Sensitive high spatial resolution ion microprobe (SHRIMP) U–Pb dating of monazite in a cordierite-gedrite basement gneiss and a quartzite indicated a protracted metamorphic event from 60 to 50 Ma (Hinchey et al., 2007), and zircon dates from migmatites pointed to a major partial melting event at ~56 Ma (Vanderhaeghe et al., 1999). In contrast, the Frigg Glacier area (F in Fig. 1), located at one of the deepest structural level of the TOD or ~2.5 km structurally below the basal quartzite, consists of basement orthogneiss folded by N–S trending folds with subhorizontal axes and subvertical axial planes that are parallel to leucosome veins (Blattner, 1971). An aplitic dyke from this locality crosscuts all structures except the N–S trending leucosome veins (Kuiper, 2003). Isotope dilution thermal ionization mass spectrometry (ID-TIMS) U–Pb dating of zircon from this dyke yielded a discordia chord with an upper and lower intercepts of 1.8 and 0.5 Ga. As discussed by Kuiper (2003), if the upper intercept represents the crystallization age of the dyke, it would imply that the core of the TOD preserves a Paleoproterozoic migmatitic gneissosity.

2.2. The Frenchman Cap dome

The FCD is divided into four structural levels termed (from top to bottom) upper cover sequence, lower cover sequence, upper basement, and lower basement (Fig. 2). All four structural levels are exposed in the moderately steep west flank, whereas the upper cover sequence is not exposed on the gently dipping, east flank. The upper cover sequence occurs immediately below the Monashee décollement, has a structural thickness of ~3 km, and comprises two fold nappes. It records east verging, penetrative ductile deformation and kyanite-K-feldspar grade metamorphism between 60 and 55 Ma (Parrish, 1995; Crowley and Parrish, 1999; Gibson et al., 1999; Crowley et al., 2001; Foster et al., 2004). The lower cover sequence has a structural thickness of ~1.5 km and comprises the upright, lower limb of the lower fold nappe. It records sillimanite-grade metamorphism and high-temperature east verging deformation until ~50 Ma, ~5 Ma later than the upper level (Crowley and Parrish, 1999; Crowley et al., 2001). The upper basement consists of Paleoproterozoic para- and orthogneisses that record penetrative Eocene deformation (Journeay, 1986; Crowley et al., 2001), whereas the lower basement consists of the same lithologic units but they do not record penetrative Cordilleran deformation (Crowley et al., 2001, 2008). We will show that the upper basement has a structural thickness of ~1.5 km and the exposed lower basement reaches a structural thickness of ~4–5 km.

2.2.1. Structural geology of the cover sequence and upper basement

Journeay (1986) mapped and conducted a structural analysis of the lower cover sequence and upper basement, and our investigation of part of the area confirmed his observations. As illustrated on Fig. 3D and 3E, a striking structural feature is the cluster of SW-plunging stretching lineations and minor fold axes that Journeay (1986) interpreted as resulting from rotation of fold axes during top-to-the-northeast shearing. It is noteworthy that such parallelism is a characteristic structural features throughout the upper and lower cover sequence levels and the ~10–15 km thick Lower Selkirk allochthon that overlies the Monashee Complex (Fig. 2; Journeay, 1986; Scammell, 1993). Other important structural features of the lower cover sequence and upper basement are northeast-verging, inclined folds that deformed the transposition foliation and lineations (referred to as F_3). These folds were only reported where the dominant transposition is easterly dipping; they are absent where the dominant transposition foliation is westerly dipping. At westerly dipping locations, the deformation is dominated by flattening, boudinage and layer-parallel shear strain (Journeay, 1986). This variation in strain pattern around the dome is key to determining the doming mechanism, as discussed below.

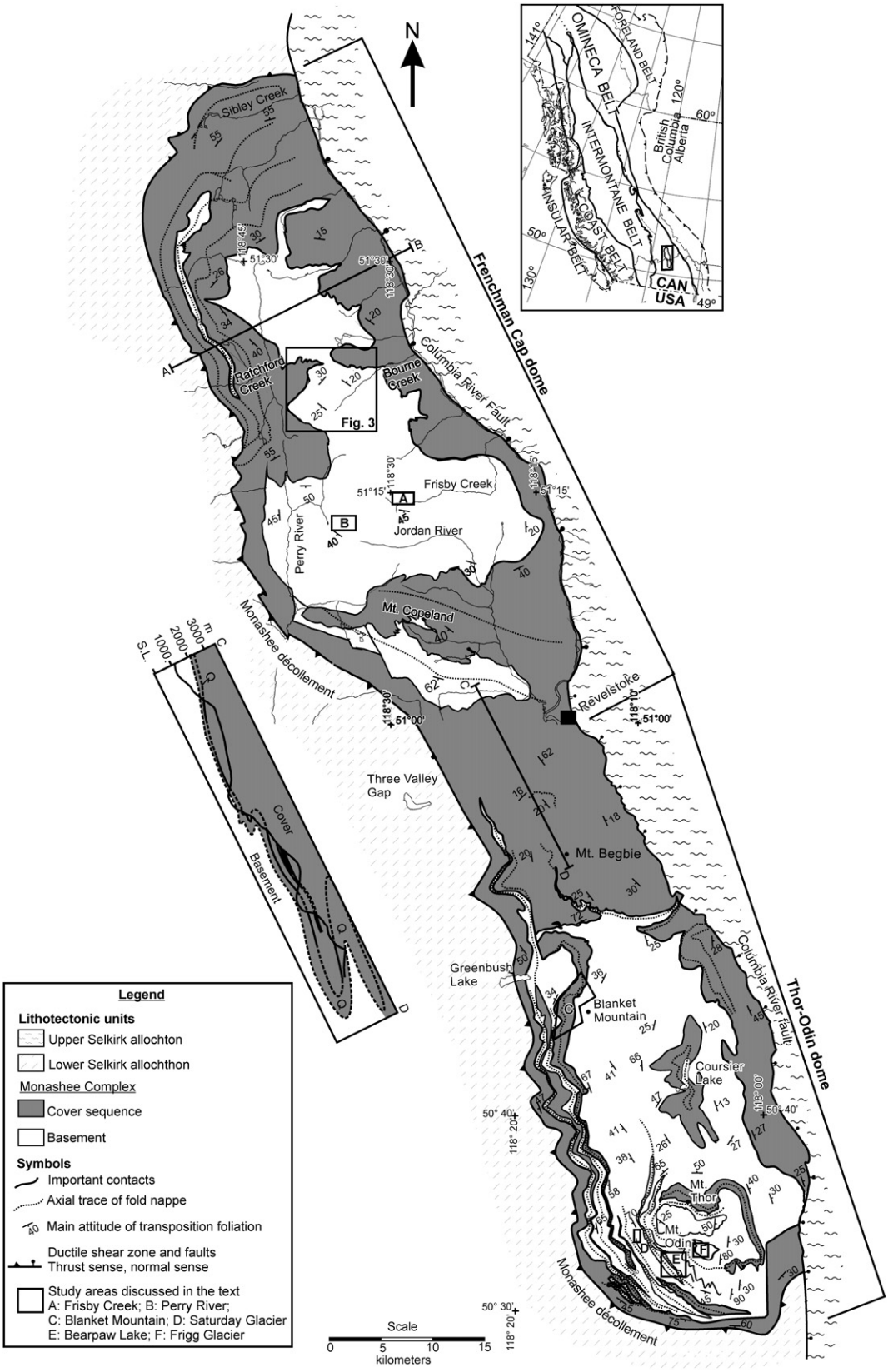

Fig. 1. Simplified geological map of the Monashee Complex. Lithologic contacts and structures from the TOD were modified from Williams and Jiang (2005). The Monashee décollement around the TOD was traced approximately parallel to the kyanite-out isograd from Johnston et al. (2000) and from Reesor and Moore (1971). Data from the FCD were modified from: Wheeler (1965), McMillan (1970), Höy and Brown (1980), Brown and Psutka (1980), Journeay (1986), Scammell (1986), Höy (1987), Gibson et al. (1999); Björnson (2003) and Gervais (2009). Cross-section C–D is modified after Read (1980). The lines are traces of mapped contacts. Q = basal quartzite. The continuity of the contacts across the domes indicates that there is no shear zone between the domes. Cross-section A–B is presented in Fig. 2. Inset shows the morphogeological map of the Canadian Cordillera (modified after Wheeler et al., 1991).

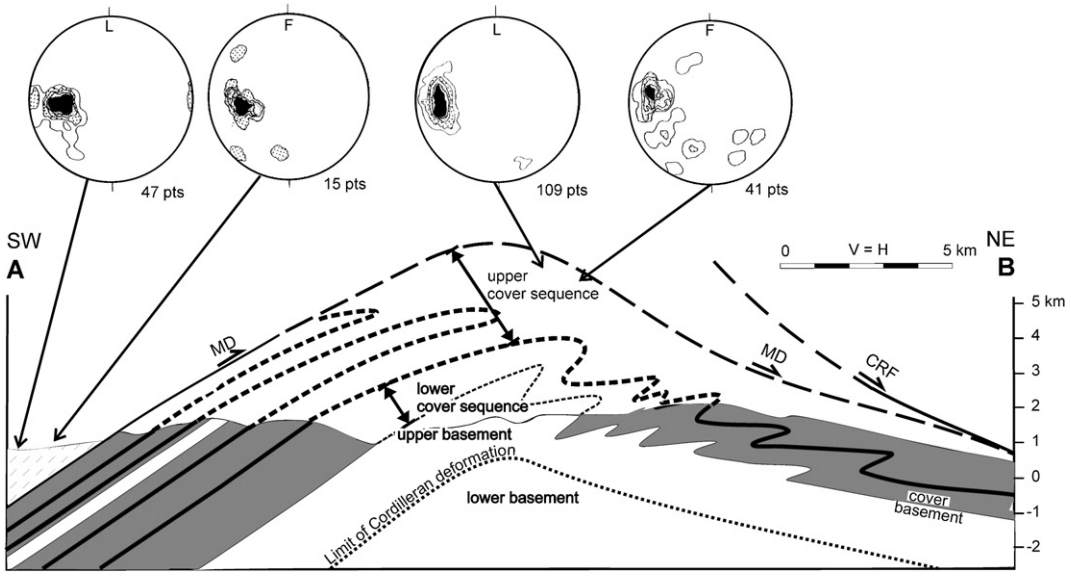

Fig. 2. SW–NE geological cross-section of the Frenchman Cap dome, with location shown as A-B in Fig. 1. The terms upper cover sequence, lower cover sequence, upper basement, and lower basement refer to structural levels discussed in text. Lower-hemisphere equal-area projections from the Lower Selkirk allochthon and the upper level of the Monashee Complex cover sequence highlight the parallelism between stretching lineation (L) and fold axes (F) indicative of a high level of strain (data from Journeay, 1986). CRF = Columbia River fault, MD = Monashee décollement. Patterns are the same as in Fig. 1.

2.2.2. Timing of metamorphism and deformation in lower cover sequence and upper basement

Timing of metamorphism and deformation in the lower cover sequence and upper basement is well constrained (Crowley and Parrish, 1999; Crowley et al., 2001). Thirty-two ID-TIMS U–Pb analyses consisting of single monazite grains or groups of grains from nine pelitic schists yielded dates between 61 and 49 Ma, with 23 analyses between 53 and 49 Ma. These results suggest that monazite started to grow during prograde metamorphism between 61 and 53 Ma and that the thermal peak was reached between 53 and 49 Ma. Timing of deformation is also tightly bracketed at these two structural levels. Foliated and boudinaged pegmatite layers that are folded by F_3 northeast-verging folds yielded concordant to slightly discordant zircon U–Pb dates of ~51 Ma that were interpreted as the crystallization age. A sheared and boudinaged sillimanite-bearing leucosome yielded concordant U–Pb dates of ~50.5 Ma, also interpreted as the crystallization age. An undeformed pegmatite, highly discordant to the gneissosity of its host basement gneiss, yielded a poorly defined linear array of zircon U–Pb analyses with a lower intercept coinciding with a concordant analysis of ~49.5 Ma, which was also interpreted as the crystallization age. As argued by Crowley et al. (2001), this dataset indicates that at least part of the transposition fabric (foliation, gneissosity, lineation, isoclinal folds) and F_3 folds developed between ~51 and 49 Ma, which coincides with the youngest period of monazite growth in pelitic schists.

2.2.3. Timing of deformation in lower basement

U–Pb geochronology of samples collected ~2 km structurally below the basement-cover contact point to a drastically different tectonic history than in the overlying rocks. Zircon and monazite from five samples from the northern toe of Bourne Glacier (area K on Fig. 3) were dated by laser ablation inductively coupled plasma mass spectrometry (LA-ICP-MS) (Crowley et al., 2008). Two samples are weakly deformed grey granite sheets that form part of a ubiquitous swarm termed the Bourne granite suite, one is an undeformed pegmatitic leucogranite dyke that is mingled with grey granite similar to that in the Bourne suite, one is an undeformed pegmatite dyke, and one is a deformed pegmatite. Zircon from all samples yielded only 1.9 Ga dates (i.e., Cordilleran zircon does not exist). In four samples, >90% of the monazite yielded ~1.9 Ga dates. One sample contains exclusively Cordilleran monazite. The possibility that all 1.9 Ga grains were inherited in Cordilleran melts was considered, yet rejected based on three tests comprising field relationships, composition and zoning of monazite and zircon, and U–Pb dates. The one sample that contains only Cordilleran monazite is a pegmatite with lobate enclaves of a grey granitic phase similar in composition and texture to the Bourne granite suite. Sixteen zircon grains were dated at 1.9 Ga, whereas 10 monazite grains yielded a weighted mean $^{206}Pb/^{238}U$ date of 50.7 ± 1.8 Ma (MSWD = 0.7), which overlaps with monazite dates from a nearby pelitic schist (Crowley, 1999). The Eocene monazite in the pegmatite was interpreted as having formed from fluids during Cordilleran metamorphism based on highly variable internal zoning and chemical composition of the grains. Another sample from a grey granite sheet from north of Bourne Creek was dated by ID-TIMS at 1.9 Ga based on an upper intercept defined by zircon and titanite analyses along a discordia line (Crowley, 1999).

By showing that weakly to undeformed granite and pegmatite crystallized at 1.9 Ga, previous work demonstrated the absence of Cordilleran penetrative ductile deformation in a relatively small (~6 × 6 km) area in the upper basement of the FCD (area covered on the map of Fig. 3). However, it remained unknown whether Cordilleran deformation is absent elsewhere in the basement of the FCD, a region that is ~10 times larger than the area studied by Crowley et al. (2008). One goal of our study was thus to assess the state of Cordilleran deformation throughout the lower basement of the FCD.

3. Bourne granite suite

Structural analysis of polydeformed terrains is not a simple task (e.g., Williams, 1985; Passchier et al., 1990; Williams et al., 2009). A useful approach is to examine the deformation state of different suites of dykes, if reliable criteria exist to link a given dyke to a specific suite. Several studies suggested that grey granite sheets within basement gneisses of the FCD are part of a ~1.9 Ga suite that

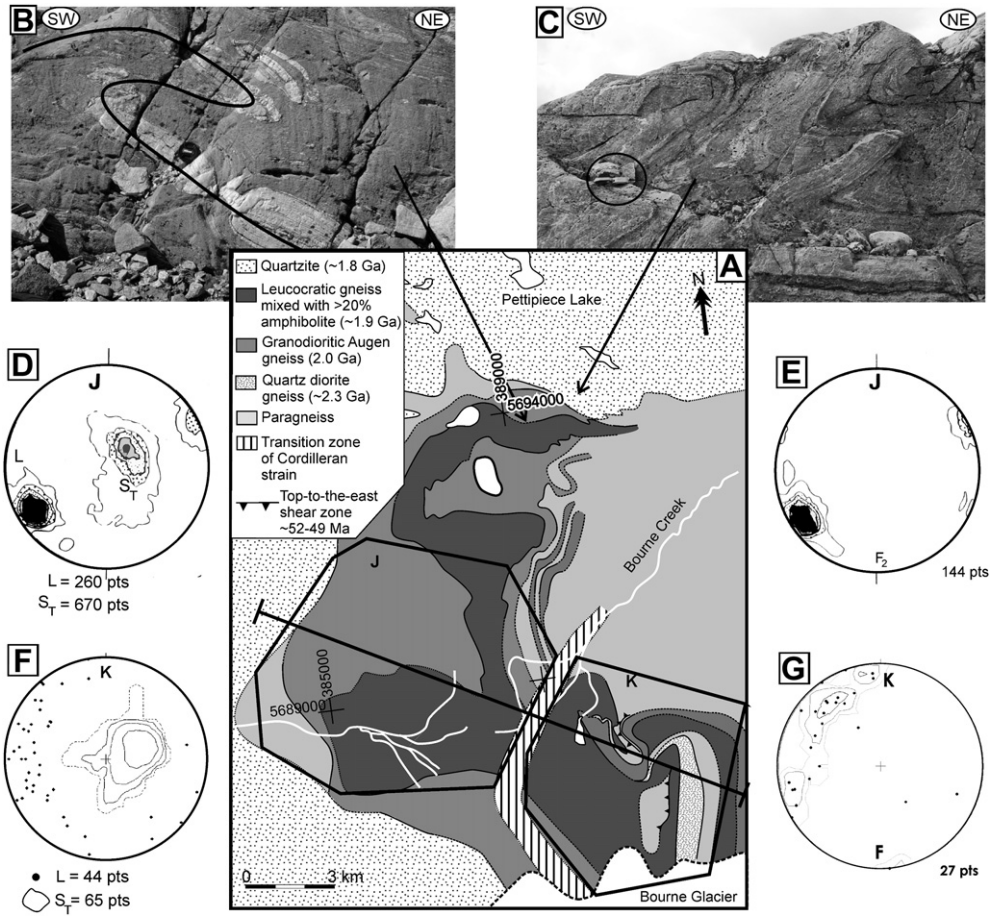

Fig. 3. Geological map, field relationships and structural data from the upper basement and lower basement at the Bourne Glacier locality. (A) Geological map. Notice the truncation of lithological units at the transition zone. Location of cross-section in Fig. 9 is shown. (B) Bourne granite dyke folded by NE-verging F_2 fold in the upper basement. (C) NE-verging, "cascading" F_2 folds (F_3 in the basement) developed in the basal quartzite of the cover sequence. Compass for scale at the left is circled. (D, E) Cordilleran deformation in the upper basement (area J on the map) is characterized by the parallelism between stretching lineations (L in D) and F_2 fold axes (F_2 in E). Data from Journeay (1986). (F, G) The spread in orientation of lineations (L in F) and fold axes (F in G) from Bourne Glacier locality (area K on the map) contrasts sharply with the clustering observed in area J. S_T = transposition foliation or gneissosity.

can be used as a time marker of deformation (Crowley, 1999; Crowley et al., 2001, 2008). However, because this conclusion was based on similar ages of only four sheets from a small area (Fig. 3), our first objective was to establish whether other grey granite sheets in different parts of the basement are part of the same ~1.9 Ga suite. All sizeable exposures of grey dykes found during ~12 weeks of fieldwork in three localities (Bourne Glacier, Perry River and Frisby Creek localities shown in Fig. 1) were collected and documented for mineral assemblages, macro- and microscopic textures, and field relationships with host gneisses. Fifteen thin-sections were examined with an optical microscope and from these, 10 were inspected with a scanning electron microscope (SEM). Four samples, including one pegmatitic leucogranite commonly associated with the grey granite, were analysed by XRF for bulk chemical composition. Zircon and titanite in one sample were dated by the U–Pb method.

3.1. Field relationships, petrography and trace elements profiles

Bourne granite is distinguished in the field by a light grey colour, a medium-grained and equigranular texture, and in the lower basement by a weak to absent alignment of mineral interpreted as a lack of solid-state fabric (Fig. 4C). It generally forms sheets 0.5–1 m thick, but veinlets 2 cm thick and stocks occupying surfaces of tens of square meters do exist. No systematic orientation of the sheets was noted. Another characteristic feature is the association between the grey granite and a coarse-grained to pegmatitic leucogranite (Fig. 4B). The pegmatitic leucogranite is commonly present at the margins of grey sheets, and heterogeneous mixing of the two phases was also observed. The common lobate contacts between these two phases and their local heterogeneous mixing are interpreted as evidence for magma mingling (Fig. 4B). At the Perry River locality, the two granitic phases are spatially correlated with lenses of ultramafic composition. In fact, the largest volume of grey granite observed in the FCD was in the aureole of a mafic–ultramafic complex, ~800 m in diameter, composed of clinopyroxenite, gabbronorite, and metagabbro. More work is needed to determine whether a co-genetic link exists between the granite and ultramafic rocks. Nevertheless, field relationships suggest that all grey granite sheets belong to one suite.

Petrographically, Bourne granite is characterized by: 1) a mineral assemblage formed by approximately 20% quartz, 25% plagioclase, 35% K-feldspar, 15% biotite, 5% allanite, and trace amounts of zircon, monazite, and titanite; 2) biotite with a very dark-colour that masks birefringence; 3) distinctive and abundant large dark-brown allanite (3–5 mm in diameter). Inspection of Bourne granite with an SEM revealed that most samples contain subhedral allanite that are zoned in rare earth elements (REE).

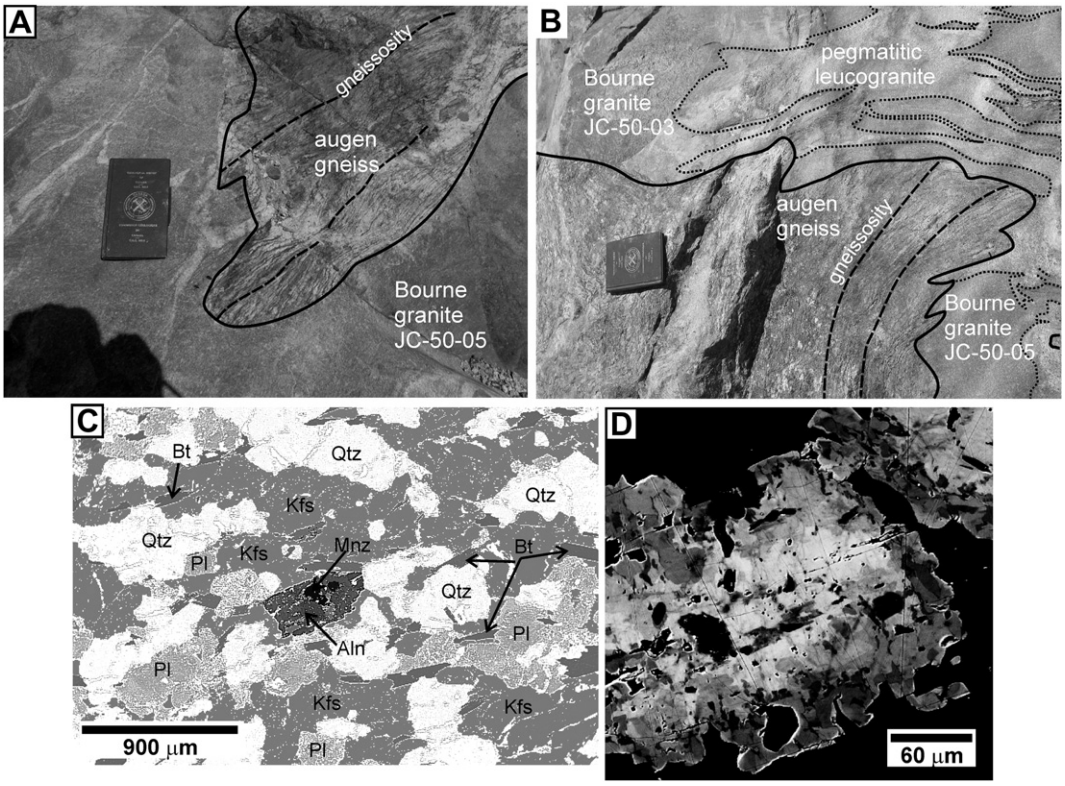

Fig. 4. Bourne granite suite. (A, B) Field relationships of dyke sample JC-50-05 from the Perry River locality. Note the high angle between the gneissosity in the host granodioritic augen gneiss and the dyke margin, and the very weak mineral alignment in Bourne granite. In (B), Bourne granite is mingled with a pegmatitic leucogranite phase. (C) Backscattered electron image (inverted colour) of a sample from the Bourne Glacier locality that was dated by Crowley et al. (2008) at ~1850 Ma. The section, which is cut parallel to the lineation and perpendicular to the foliation of the host gneiss, shows that quartz (white) is clearly not aligned and has a euhedral to subhedral shape. Also shown is the typical allanite corona surrounding resorbed magmatic monazite. (D) Backscattered electron image of allanite in sample FG-425b-05 from the Frisby Creek locality. See text for interpretations. Abbreviations: Bt = biotite; Pl = plagioclase; Kfs = K-feldspar; Mnz = monazite; Aln = allanite.

REE-rich cores are surrounded by REE-poor rims (Fig. 4D), perhaps indicating a magmatic origin (e.g., Beard et al., 2006). In contrast, some sheets contain oscillatory-zoned monazite as a magmatic phase instead of allanite (Crowley et al., 2008). Monazite in these dykes is generally rimmed by complex corona consisting of allanite ± apatite, thorite and phengite (Fig. 4C). The presence of magmatic monazite in some grey granites and magmatic allanite in others could indicate that they belong to two distinct suites or reflect a more calcic composition for the allanite-bearing dykes (Cuney and Friedrich, 1987; Dini et al., 2004). Thus, determining if both types of grey granites belong to the same suite is important.

Three grey granite sheets, one from each locality investigated in the lower basement (Bourne Glacier, Perry River and Frisby Creek), and one pegmatitic leucogranite mingled with a grey granite phase (from Perry River locality) were analysed by XRF for trace elements profiles (Table 1). The three grey granites have the same trace element profiles and the white leucogranite has peaks and troughs for the same elements as those of the grey granite (Fig. 5). Although this dataset is limited, it supports the hypothesis that grey granites from three different localities in the lower basement are from the same suite.

3.2. U–Pb geochronology

3.2.1. Analytical methods

Zircon and titanite grains were isolated using standard mineral separation techniques. Grains were mounted in epoxy and polished to reveal their centres. Cathodoluminescence (CL) imaging was conducted at Carleton University with an Electron Optics Services system interfaced to the Camebax microprobe, consisting of a high sensitivity photo-multiplier (PM) tube connected to a Baush and Lomb CL amplifier. Images were collected at 15 kV accelerating potential and 15 nA beam current. Backscattered electron (BSE) images of the polished titanite were acquired with an electron microprobe (EMP) at the Massachusetts Institute of Technology with a JEOL 733 Superprobe, with an accelerating voltage of 15 keV and beam current of 30 nA.

Isotopic data were acquired by laser ablation – multiple collector – inductively coupled plasma – mass spectrometry (LA-MC-ICP-MS) at the radiogenic isotope facility (RIF) of the University of Alberta, Edmonton. Instrumentation includes a Nu Plasma MC-ICP-MS, coupled to a Nd:YAG UP213 laser ablation system. The MC-ICP-MS instrument is equipped with a modified collector block containing 12 F collectors and three ion counters (Simonetti et al., 2005). Raw data were normalized against the zircon standard FC-1 (~1098 Ma) and titanite standard Khan (~521 Ma; Simonetti et al., 2006). Additional analytical protocol and instrumentation is described in Simonetti et al. (2006). Errors are given at 2σ. Plots were made with Isoplot3 (Ludwig, 2008). Using a 40 × 40 μm laser spot typically provided space for one or two analyses per grain. For a few analyses of small areas, labelled with asterisks in Tables 2 and 4, a 20-μm laser spot was used.

Because few studies have used LA-ICP-MS to date titanite, it is important to evaluate the accuracy and precision obtained on the standard BLR-1, dated by Aleinikoff et al. (2007) at 1047.1 ± 0.4 Ma, which was routinely analysed along with the unknowns. Three methods exist to correct for the large amount of common Pb typically present in titanite (Aleinikoff et al., 2004; Storey et al.,

Table 1
Major and trace elements compositions.

Sample	JC-33-05	JC-50-05	FG-425b-05	FG-187-04
Rock type	Leuco-granite	Bourne granite	Bourne granite	Bourne granite
Locality	Perry River	Perry River	Frisby Creek	Bourne Glacier
UTM NAD83 Zone 11	390288E 5686655N	389458E 5675424N	394005E 5677681N	390387E 586506N
Major elements (weight %)				
SiO2	77.26	72.2	72.94	70.44
Al2O3	12.65	13.44	13.27	13.77
CaO	2.44	1.39	1.3	1.73
Fe2O3(T)	2.05	3.26	2.51	3.68
K2O	0.67	5.8	6.16	5.67
MgO	0.13	0.32	0.33	0.43
MnO	0.03	0.05	0.03	0.04
Na2O	4.33	2.66	2.54	2.6
P2O5	0.02	0.06	0.08	0.07
TiO2	0.08	0.26	0.32	0.33
L.O.I.	0.70	0.80	0.80	0.30
Sum	99.80	99.65	99.77	99.04
Trace elements (ppm)				
Ba	77	830	1582	948
Ce	84	234	278	333
Co	5	4	3	6
Cr	14	24	12	12
Ga	21	18	16	20
La	49	107	115	188
Nb	13	21	12	25
Nd	39	81	92	120
Ni	27	58	19	17
Pb	20	58	37	47
Rb	33	155	216	225
Sr	354	212	165	153
Th	53	61	37	65
U	16	6	3	7
V	7	7	16	19
Y	43	32	16	25
Zn	32	50	44	57
Zr	592	242	304	355

2006). The first regresses the uncorrected data on a Tera–Wasserburg semi-total Pb plot. If the data form an isochron, the intercept on the *y*-axis is assumed to yield the initial common Pb ratio, whereas the lower intercept on the concordia curve yields the age of the titanite. The second method calculates the weighted mean average of individual $^{206}Pb/^{238}U$ dates corrected with the *Age7corr* algorithm in Isoplot3 (Ludwig, 2008), using the *y*-intercept on the Tera–Wasserburg plot and its uncertainty for the common Pb correction. If the analyses do not yield an isochron, the common Pb can be estimated from Stacey and Kramers (1975). The second and third methods have the disadvantage of assuming concordancy of the analyses, but yield better precision. Discarding one of the 11 analyses of BLR-1 standard, which was clearly off the regression line on the Tera–Wasserburg plot, yielded an age of 1041 ± 110 Ma (MSWD = 0.79; prob. = 0.62) for the first method and a weighted mean average of 1043 ± 35 Ma (MSWD = 0.09; prob. = 1.00) for the second method, both in agreement with the true age.

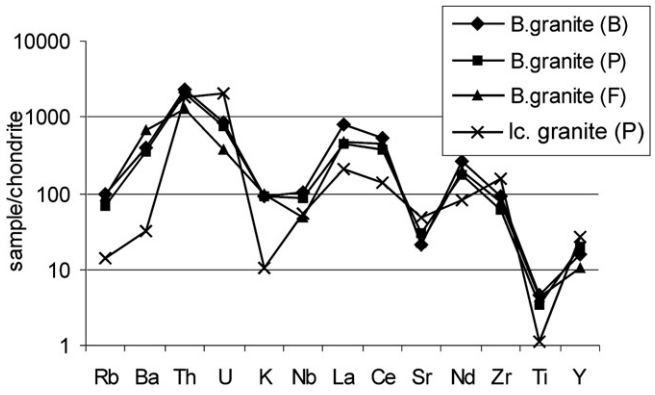

Fig. 5. Trace element profiles for Bourne granite highlight the similarities between three Bourne granite samples from each of the three studied localities. B.granite = Bourne granite from: 1) B = Bourne Glacier, sample FG-187-04; 2) P = Perry River, sample JC-50-05; F = Frisby Creek, sample FG-425b-05. lc. granite (P) = leucogranite sample JC-33-05 from Perry River.

3.2.2. Results

Grey granite sample JC-50-05 was collected at the Perry River locality. At the collection site, the grey granite is heterogeneously mixed with pegmatitic leucogranite (Fig. 4B) and lenses of ultramafic igneous rocks, which together form a stock a few tens of meters wide. In the field, the grey granite appears to have a lineation defined by aligned K-feldspar, but under the microspcope it has an equigranular texture with equant grains of quartz, similar to the inverse-coloured SEM picture of Fig. 4C. Importantly, the sample lacks monazite, but contains rare titanite in mm-scale isolated leucocratic pockets, as well as ~5% allanite that is euhedral to subhedral, zoned in REE, and has a resorbed texture at grain margins (Fig. 4D). Inasmuch as allanite microtextures are interpreted as evidence of a magmatic origin, sample JC-50-05 constitutes an ideal candidate to determine whether allanite-bearing grey granites are related to the monazite-bearing grey granites dated elsewhere.

CL images reveal that zircon is generally sector or oscillatory zoned (Fig. 6B), with the zoning commonly being blurred. CL images also show thin black rims around most grains (Fig. 6B, C). Eight $^{207}Pb/^{206}Pb$ dates between 1940 and 2100 Ma are interpreted as being from inherited components (Table 2). Twelve other dates are discordant (7–19%) and define a linear array (MSWD = 2.3; prob. = 0.01) with an upper intercept of 1861 ± 58 Ma and a lower intercept of 344 ± 400 Ma (Fig. 6A; Table 2). A 20-μm laser spot was used to analyse the thin black rims seen in the CL images on many grains, in our sample and the grey granite samples examined by Crowley et al. (2008). Two black rims yielded dates indistinguishable from dates obtained on spots from oscillatory-zoned zircon (Fig. 6C, Table 2), confirming that no parts of the grains are Tertiary. The upper intercept date of 1861 ± 58 Ma is interpreted as the igneous crystallization age, and the overlap with dates obtained by Crowley et al. (2008) on Bourne granite samples indicates that our sample is part of the suite.

Five titanite grains from sample JC-50-05 were dated (Fig. 7; Table 3). The grains commonly have a diameter of ~500 μm, are subhedral and have patchy zoning with some planar zoning that could be considered as relict oscillatory zoning (Fig. 7A and B). Using the Stacey and Kramers (1975) method for common Pb correction at 1850 Ma, three analyses from one titanite grain yielded dates of ~1707, 1715 and 1399 Ma. This grain is interpreted as having formed during Paleoproterozoic crystallization of the granite and retained most of its Pb through Cordilleran metamorphism. Other analyses are younger and were treated with the other methods for common Pb correction (see above). Regression of six uncorrected analyses from four grains on a Tera–Wasserburg plot yields a lower intercept of 49.2 ± 2.6 Ma (MSWD = 5.3; prob. fit = 0.0) and a *y*-axis ($^{207}Pb/^{206}Pb$) intercept of 0.82 ± 0.05. Using the *y*-axis value of $^{207}Pb/^{206}Pb$ for common Pb correction yields a corrected weighted mean average $^{206}Pb/^{238}U$ age of 49.3 ± 1.1 Ma (MSWD = 0.90; prob. fit = 0.48). The presence of Paleoproterozoic radiogenic Pb in one titanite grain suggests that they grew during this period and that Pb diffusion in the Eocene was not complete in all grains. The ~49 Ma age is therefore interpreted as the time at which these titanite grains closed to Pb diffusion after limited (either in time or temperature) Eocene heating.

Table 2
U–Pb LA-MC-ICP-MS analyses of zircon from Bourne granite sample JC-50-05 (Perry River locality).

Anal.#	$^{207}Pb/^{206}Pb$	$\pm 2\sigma$	$^{207}Pb/^{235}U$	$\pm 2\sigma$	$^{206}Pb/^{238}U$	$\pm 2\sigma$	rho	$^{207}Pb/^{206}Pb$ date (Ma)	$\pm 2\sigma$ (Ma)
JC-50-05 from the Perry River locality UTM 389458E – 5675424N (Zone 11)									
Igneous									
L01-1	0.11283	0.00120	4.2059	0.1264	0.2704	0.0108	0.99	1845	19
L03-1	0.11335	0.00119	4.7414	0.1423	0.3034	0.0101	0.95	1854	19
L04-1	0.11075	0.00114	4.3862	0.1317	0.2872	0.0099	0.96	1812	19
L05-1	0.11089	0.00111	4.2827	0.1287	0.2801	0.0115	0.73	1814	18
L06-1	0.11287	0.00116	4.3997	0.1321	0.2827	0.0105	0.98	1846	19
L09-1	0.11047	0.00113	4.0772	0.1226	0.2677	0.0110	0.73	1807	19
L10-1	0.10900	0.00110	4.0762	0.1223	0.2712	0.0087	0.95	1783	18
L12-1	0.10974	0.00111	4.0086	0.1203	0.2649	0.0088	0.95	1795	18
S_10	0.11013	0.00122	4.4591	0.1338	0.2937	0.0094	0.94	1802	20
S-27	0.11195	0.00118	3.9921	0.1203	0.2586	0.0139	0.56	1831	19
S-30[a]	0.11316	0.00125	4.6192	0.1391	0.2961	0.0154	0.58	1851	20
S-34	0.11136	0.00114	4.1080	0.1233	0.2675	0.0082	0.94	1822	19
Inherited									
L15-1	0.11915	0.00155	4.9633	0.1489	0.3021	0.0094	0.91	1943	23
S_01	0.12997	0.00177	6.4141	0.1925	0.3579	0.0111	0.90	2098	24
S_04	0.12194	0.00143	5.7060	0.1712	0.3394	0.0108	0.93	1985	21
S_15	0.12104	0.00144	5.9049	0.1772	0.3538	0.0109	0.92	1972	21
S-11	0.12496	0.00134	5.4948	0.1649	0.3189	0.0102	0.94	2028	19
S-18	0.12598	0.00138	5.8682	0.1761	0.3378	0.0108	0.94	2043	19
S-22[a]	0.12333	0.00140	5.1223	0.1543	0.3012	0.0164	0.55	2005	20
S-26	0.12423	0.00137	5.3096	0.1594	0.3100	0.0105	0.95	2018	20
L02-1	0.12619	0.00130	5.5690	0.1672	0.3201	0.0113	0.96	2046	18

[a] Black rims on cathodoluminescence images.

3.3. Interpretation

Our results demonstrate that grey granite intrusions in the basement gneisses of the FCD are of part of the Paleoproterozoic Bourne suite. Five grey granite sheets and two pegmatite dykes are dated with crystallization ages of ~1850 Ma (Fig. 8). Combining the dates yields a weighted mean $^{207}Pb/^{206}Pb$ age of 1850 ± 4 Ma (MSWD = 0.94; prob. = 0.45). The dated samples cover the entire spectrum of grey granite types including monazite-bearing grey granite, monazite rimmed by allanite-bearing grey granite, allanite-bearing grey granite mingled with a pegmatitic leucogranite and ultramafic lenses, pegmatitic white granite including lobate enclaves of grey granite, and a stock of titanite-bearing grey granite. The granites occur in various locations in the upper and lower basement of the FCD (Fig. 1). Similar REE profiles from three grey granite samples from three locations in the lower basement, including sample JC-50-05 dated herein and one pegmatitic leucogranite mingled with a grey granitic phase, suggest that all grey granites share a similar chemical composition. Bourne granite sheets are easily identified in the field by grey colour, equigranular and medium-grained texture, discordant relationship with the gneissosity in the host gneiss, and a common association with a pegmatitic leucogranite. Microscopically, Bourne granite is characterized by the presence of zoned allanite or by coronas of allanite surrounding resorbed monazite, and by a very dark biotite that masks birefringence. Consequently, macroscopic, microscopic, geochemical, and most importantly geochronologic data demonstrate that grey granite dykes that intruded basement gneisses of the FCD are part of a ~1850 Ma plutonic suite. Furthermore, preservation of Paleoproterozoic radiogenic Pb in titanite strongly suggests that the Bourne suite was not heated significantly until a few millions of years before ~49 Ma. These results entirely support the previous conclusion that structures older than the Bourne granite are Paleoproterozoic. Younger structures could also be Paleoproterozoic, but are more likely related to Cordilleran tectonism, and thus are probably Eocene. Bourne granite dykes therefore constitute very useful time markers of deformation.

4. Lithologic units in upper and lower basement

4.1. Field investigation

Most of the FCD was mapped at least at the 1:50,000 scale and its structural geometry is well characterized (McMillan, 1970; Fyles, 1970; Brown and Psutka, 1980; Höy and Brown, 1980; Journeay,

Table 3
U–Pb LA-MC-ICP-MS analyses of titanite from Bourne granite sample JC-50-05 (Perry River locality).

	Uncorrected isotopic ratios and uncertainties					Corrected age[a]	
	$^{207}Pb/^{206}Pb$	$\pm 2\sigma$	$^{238}U/^{206}Pb$	$\pm 2\sigma$	rho	$^{238}U/^{206}Pb$ (Ma)	$\pm 2\sigma$
M04_1	0.1235	0.0013	3.2269	0.1142	0.98	1707	59
M04_2	0.1393	0.0016	3.8906	0.1293	0.98	1399	45
M04_3	0.1232	0.0012	3.2133	0.1016	0.98	1715	53
M12_1	0.7391	0.0126	11.9103	0.5287	0.82	58	32
M13_1	0.3677	0.0056	74.7463	2.7583	0.82	50	3
M13_2	0.3807	0.0061	74.9314	2.4994	0.82	49	3
M14_1	0.1708	0.0023	109.3354	3.7372	0.82	49	2
M14_2	0.1917	0.0056	105.2591	4.3419	0.82	50	2
M18_1	0.5033	0.0087	58.7494	2.0252	0.82	45	5

[a] Common Pb used to correct the age was estimated from Stacey and Kramers (1975) for grain M4 and from the *y*-intercept on the Tera–Wasserberg plot (Fig. 7) for all other analyses.

Table 4
U–Pb LA-MC-ICP-MS analyses of zircon from leucosome samples (lower basement).

Anal.#[a]	$^{207}Pb/^{206}Pb$	$\pm 2\sigma$	$^{207}Pb/^{235}U$	$\pm 2\sigma$	$^{206}Pb/^{238}U$	$\pm 2\sigma$	rho	Date[b] (Ma)	$\pm 2\sigma$ (Ma)
JC-42-05 from the Perry River locality UTM 389458E – 5675424N (Zone 11)									
L02-1	0.12619	0.00130	5.5690	0.1672	0.3201	0.0113	0.96	2046	18
L04-1	0.12579	0.00128	5.5340	0.1662	0.3191	0.0119	0.98	2040	18
L05-1	0.12508	0.00129	5.4020	0.1621	0.3132	0.0105	0.95	2030	18
L09-1	0.12487	0.00126	5.4612	0.1639	0.3172	0.0109	0.96	2027	18
L11-1	0.12586	0.00133	5.5366	0.1662	0.3190	0.0119	0.97	2041	19
M-1	0.12580	0.00132	5.3383	0.1602	0.3078	0.0106	0.96	2040	19
M-11	0.12663	0.00132	5.5267	0.1659	0.3165	0.0115	0.97	2052	18
M-12	0.12563	0.00130	5.3646	0.1610	0.3097	0.0109	0.96	2038	18
M-13	0.12625	0.00128	5.4987	0.1650	0.3159	0.0105	0.95	2046	18
M-14	0.12344	0.00128	5.1350	0.1542	0.3017	0.0109	0.97	2007	18
M-16	0.12602	0.00128	5.1422	0.1543	0.2959	0.0095	0.95	2043	18
M-17	0.12737	0.00131	5.7227	0.1717	0.3259	0.0109	0.95	2062	18
M-18	0.12674	0.00128	5.6496	0.1696	0.3233	0.0108	0.95	2053	18
M-2	0.12560	0.00129	5.4596	0.1640	0.3153	0.0123	0.99	2037	18
M-20	0.12665	0.00129	5.6484	0.1696	0.3235	0.0123	0.98	2052	18
M-21	0.12420	0.00126	5.2965	0.1590	0.3093	0.0113	0.97	2017	18
M-22	0.12665	0.00130	5.5262	0.1659	0.3164	0.0110	0.96	2052	18
M-2-3	0.12676	0.00129	5.6911	0.1708	0.3256	0.0115	0.96	2054	18
M-3	0.12795	0.00130	5.8741	0.1763	0.3330	0.0117	0.96	2070	18
M-5	0.12558	0.00129	5.3982	0.1621	0.3118	0.0112	0.97	2037	18
M-8	0.12685	0.00129	5.5931	0.1679	0.3198	0.0116	0.97	2055	18
M-9	0.12646	0.00128	5.4717	0.1643	0.3138	0.0117	0.98	2049	18
FG-425c-05 from the Frisby Creek locality UTM 394005E – 5677681N (Zone 11)									
Inherited									
M01-1	0.12333	0.0012	5.3082	0.1594	0.3122	0.0115	0.98	2005	18
M02-1	0.12616	0.0013	5.3490	0.1605	0.3075	0.0104	0.95	2045	19
M03-1	0.12517	0.0013	5.3551	0.1608	0.3103	0.0114	0.97	2031	18
M04-1	0.12671	0.0021	5.8128	0.1745	0.3327	0.0111	0.86	2053	30
M04-2	0.12246	0.0013	4.6956	0.1410	0.2781	0.0097	0.96	1992	19
M05-1	0.12733	0.0013	5.6746	0.1704	0.3232	0.0115	0.96	2061	18
M05-2	0.12578	0.0013	5.5441	0.1664	0.3197	0.0111	0.96	2040	18
M06-1	0.12550	0.0013	5.0017	0.1502	0.2891	0.0105	0.97	2036	18
M07-1	0.12736	0.0013	5.8605	0.1759	0.3337	0.0111	0.95	2062	18
M07-2	0.12393	0.0014	4.8923	0.1468	0.2863	0.0089	0.93	2014	21
M08-1	0.12530	0.0014	5.4179	0.1626	0.3136	0.0099	0.93	2033	20
M10-1	0.12666	0.0013	5.4389	0.1632	0.3114	0.0106	0.96	2052	18
M12-1	0.12628	0.0013	5.6572	0.1698	0.3249	0.0110	0.96	2047	18
Igneous									
S10-1	0.04714	0.00449	0.0539	0.0049	0.0083	0.0003	0.01	53	2
S10-2*	0.03522	0.00129	0.0399	0.0020	0.0082	0.0003	0.70	53	2
S10-3*	0.03825	0.00094	0.0426	0.0019	0.0081	0.0004	0.84	52	2

[a] 40 × 40 μm laser beam size except for * that were 20 × 20 μm.
[b] Dates are $^{207}Pb/^{206}Pb$ for Precambrian date and $^{206}Pb/^{238}U$ for Tertiary dates.

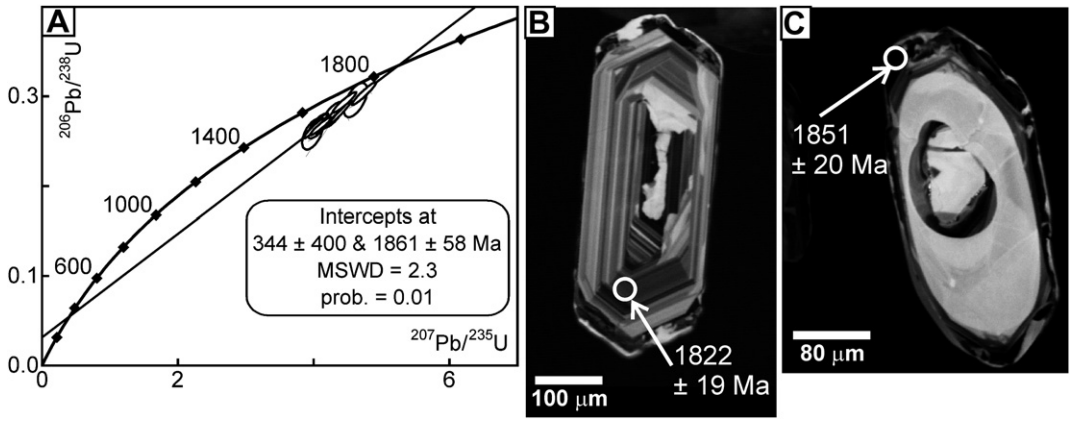

Fig. 6. LA-MC-ICP-MS zircon U–Pb geochronology of Bourne granite sample JC-50-05 from the Perry River locality. (A) Concordia plot showing a discordia with upper and lower intercepts of 1861 ± 58 Ma and 344 ± 400 Ma, respectively (MSWD = 2.3). Upper intercept is interpreted as the crystallization age. Error ellipses plotted at 2σ. Plotted with Isoplot3 (Ludwig, 2008). MSWD = Mean Square of Weighted Deviates. prob. = probability of fit. (B) Cathodoluminescence (CL) image of zircon showing oscillatory zoning, dark rim, and location of analysis spot with $^{207}Pb/^{206}Pb$ date (error is 2σ). (C) CL image of zircon showing that the dark rims common to many grains of the suite are Paleoproterozoic.

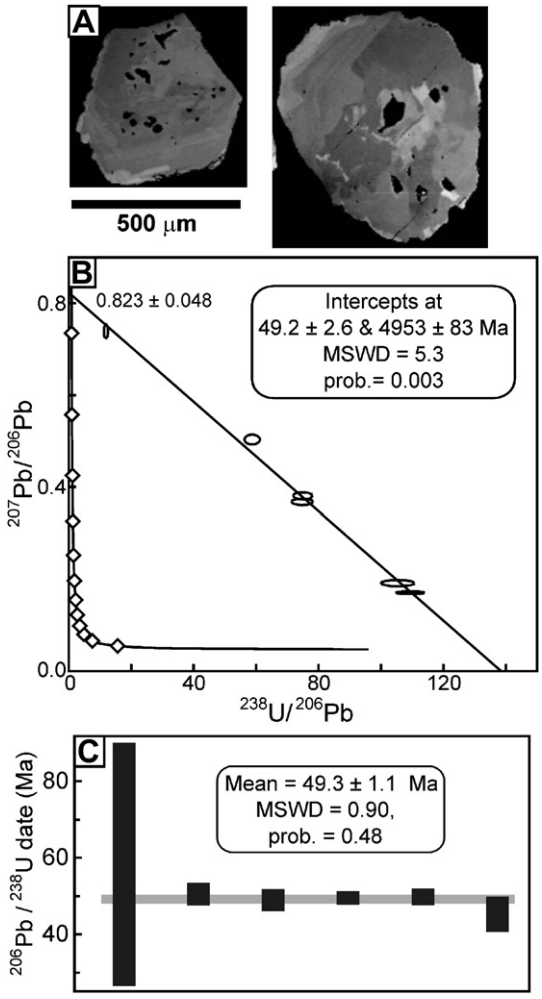

Fig. 7. LA-MC-ICP-MS titanite U–Pb geochronology of Bourne granite sample JC-50-05 from the Perry River locality. (A). BSE images of titanite with subhedral shape and zoning that could be interpreted as relict oscillatory zoning. (B) Tera–Wasserburg plot for the youngest analyses. Upper intercept on the *y*-axis is interpreted as the initial common Pb composition and lower intercept on concordia curve yields an age of 49.2 ± 2.6 Ma (error is 2σ). (C) Weighted mean $^{206}Pb/^{238}U$ age of 49.3 ± 1.1 Ma (error is 2σ) corrected for common Pb by using the *y*-intercept in (C) as the initial common Pb (Aleinikoff et al., 2004; Storey et al., 2006). The ~49 Ma age is interpreted as the time at which these titanite grains closed to Pb diffusion. (B) and (C) were plotted with Isoplot3 (Ludwig, 2008). MSWD = Mean Square of Weighted Deviates. prob. = probability of fit.

1986; Höy, 1987; Lane et al., 1989; Scammell, 1986; Gibson et al., 1999; Björnson, 2003). An exception is the lower basement that was only mapped at the 1:253,440 scale by Wheeler (1965). Four superbly exposed areas were investigated during this study (Fig. 1). The Bourne Glacier, Perry River, and Frisby Creek localities are located structurally below the cover-basement contact by approximately 1.5–3, 4–5, and 6–7 km, respectively. Fieldwork in the upper basement consisted of comparing finite strain patterns and deformation history between cover and basement rocks along the contact that is well exposed south of Pettipiece Lake (Fig. 3). The 1:50,000 map of the upper basement (Journeay, 1986) was extended southward to encompass the areas north of Bourne Glacier where Crowley et al. (2001, 2008) collected samples for U–Pb dating (area K on Fig. 3A). The complicated geology of the Perry River and Frisby Creek localities was not mapped in detail; fieldwork in these areas rather focused on documenting intrusive relationships between Bourne granite dykes and their host gneisses.

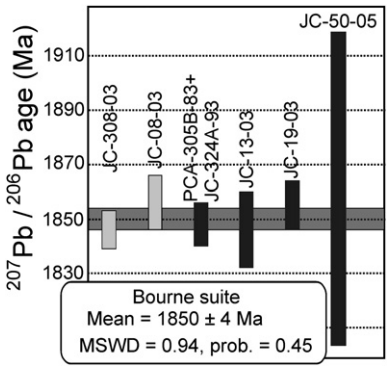

Fig. 8. Plot of $^{207}Pb/^{206}Pb$ dates from samples of Bourne granite (black boxes) and pegmatite (light grey boxes). The weighted mean age of the suite is shown (error is 2σ). The age of samples: 1) with end digits 83 and 93 were published in Crowley (1999); 2) with end digits 03 were published in Crowley et al. (2008); and 3) with end digits 05 are from this study.

4.2. Lithologic units

South of Pettipiece Lake (Fig. 3A), the cover sequence consists of a 500–1000 m thick layer of basal quartzite containing a varying amount of muscovite (5–20%) and the underlying basement is dominated by orthogneiss. The oldest lithologic units are ~2.2 Ga quartz diorite and >2.1 Ga paragneiss (Crowley, 1999). These two units crop out as rafts, lenses and slivers within a ~2.1 Ga (Crowley, 1999) biotite–hornblende ± garnet granodioritic augen gneiss (unit 2d of Journeay, 1986) that constitutes the volumetrically dominant unit throughout the basement. The volume of leucosome and the strain level of the augen gneiss are variable. Accordingly, mapping of outcrops identified as unit 2c in Journeay (1986) revealed that this unit is more likely a zone of more deformed augen gneiss rather than a different unit, and thus units 2c and 2d were regrouped into one "granodioritic augen gneiss" unit on Fig. 3A. The alaskitic gneiss units 2a and 2b of Journeay (1986), consisting of leucocratic gneiss containing more and less than 20% amphibolite, respectively, were regrouped into a single unit on the map of Fig. 3A. Crosscutting relationships indicate that amphibolites are mafic dykes that were intrusive in the leucogranitic gneiss. It was possible to map these units at Bourne Glacier (Fig. 3A), but not at Frisby and Perry River localities because their interlayering at the meter-scale would have required mapping at a scale <1:5000.

5. Structural geology of the upper and lower basement

5.1. Upper basement: south of Pettipiece Lake

Numerous studies demonstrated that rocks of the cover sequence only underwent Cordilleran deformation and metamorphism (Parrish, 1995; Crowley and Parrish, 1999; Gibson et al., 1999; Crowley et al., 2001; Foster et al., 2004). Deformation of the basal quartzite can thus be compared with that of basement gneiss to qualitatively determine the extent of Cordilleran deformation in the basement. In the relatively small area examined here, we consider it best to use a sequential notation of deformation F_1, F_2… to compare the deformation history of basement and cover rocks. The use of this notation scheme does not imply that folds belong to distinct deformation events, because we acknowledge that deformation was most likely progressive and involved rotation of fold axes toward the direction of maximum elongation (e.g., Hanmer and Passchier, 1991).

South of Pettipiece Lake (Fig. 3A), laminations and bedding in the basal quartzite were isoclinally folded by F_1 folds. F_1 imparted

a penetrative foliation dipping generally to the NE, and a strong NNE-plunging lineation. S_1 foliation was folded by NE-verging F_2 folds characterized by a gently dipping long limb and a steeply dipping short limb, an axial plane with a steeper dip than the foliation, and a fold axis trending NW–SE (Fig. 3C). This type of fold has often been referred to as "cascading" and reported elsewhere as F_3 (e.g. Brown and Psutka, 1980; Journeay, 1986; Höy, 1987). Basement rocks, including Bourne granite dykes, share the same deformation history as the basal quartzite except that an earlier foliation was folded by the first set of isoclinal folds. F_1 in the cover is thus F_2 in the basement. Bourne granite dykes are commonly oblique to an early foliation, but are intensely folded, foliated, and lineated (Figs. 3B and 9A). Journeay (1986) mapped this area, as well as the adjacent area labelled "J" in Fig. 3A, where the westerly dip of the regional foliation allows a direct comparison with area K in the lower basement. Lower-hemisphere, equal-area projections from area J highlight the co-linearity between SW-plunging stretching lineations (L on Fig. 3D) and F_2 fold axes (Fig. 3E). The co-linearity is indicative of a high level of strain (Williams and Jiang, 2005) that is common to all overlying high-grade rocks of the Monashee Complex and Lower Selkirk allochthon at the latitude of the FCD (Fig. 2; Journeay, 1986; Scammell, 1986, 1993; Gibson et al., 1999; Johnson, 2006).

5.2. Transition zone

The finite strain patterns change abruptly at the head of Bourne Creek. The truncation of layers of augen granodioritic orthogneisses and paragneisses that are N–S striking north of Bourne creek near the precipitous outcrops surrounding Bourne Creek (Fig. 3A), suggest a structural break. There, basement orthogneisses are not much lineated but are deformed by abundant easterly verging folds (Fig. 9B) with a variable attitude of axial planes and fold axes interpreted as reflecting different degree of fold rotation during east-directed shearing. We argue that this area is a transition zone, approximately 600 m thick, between the upper basement orthogneisses that record penetrative Cordilleran strain (Fig. 9A) and the lower basement orthogneisses that do not.

5.3. Lower basement: Bourne Glacier

Basement rocks located structurally below the transition zone at the toe of Bourne Glacier show quite different structural style than rocks above. The main lithologic unit is the same granodioritic augen gneiss present in the upper basement, but with less deformation. Cores of primary K-feldspar megacrysts are commonly preserved in the lower basement, whereas they are entirely recrystallized in the upper basement (compare Fig. 9A with Fig. 9C). Rims of these primary megacrysts were recrystallized into augen that are slightly stretched, but not as much as the long cigar-shaped augen commonly observed in the upper basement. Folds generally postdate the gneissosity, are upright and symmetric with axes plunging gently toward the northwest, although some rare recumbent folds were observed (Fig. 10). Importantly, Cordilleran-type folds were not observed in the lower basement. Such folds vary between isoclinal with axes and axial surfaces rotated into sub-parallelism with the lineation and foliation, respectively, and post-foliation, northeast-verging folds with axial surface dipping steeply to the west. The stark contrast between the two structural levels is best illustrated on lower-hemisphere equal-area projections of fold axes and lineations (stretching and mineral). Lineations from Bourne Glacier spread in a $>180^\circ$ girdle (Fig. 3F), whereas those from the upper basement cluster in the southwest quadrant (Fig. 3D). Fold axes from Bourne Glacier form a girdle within the northwest quadrant (Fig. 3G), whereas those from the upper basement cluster in the southwest quadrant, parallel to lineations (Fig. 3E).

The limited extent of Cordilleran deformation at Bourne Glacier is clearly indicated by the deformation state of the Bourne granite sheets and dykes. They are generally highly discordant to the gneissosity in their host (Fig. 9G) and crosscut limbs of folds at a high angle (Fig. 9F). They are also weakly deformed and exhibit only a weak mineral alignment (Fig. 4C). Crowley et al. (2008) showed that the migmatitic foliation formed between ~1925 Ma, the age of an isoclinally folded leucocratic layer lying axial-planar to the layering (Fig. 10), and ~1850 Ma, the age of Bourne granite dykes that crosscut a transposition fabric at a high angle within the same outcrop.

5.4. Lower basement: Perry River and Frisby Creek localities

Kuiper et al. (2006) suggested that rocks at the Bourne Glacier locality were within a mega-scale boudin surrounded by rocks recording high Cordilleran strain. To test this hypothesis, we investigated the two best-exposed localities in the deepest structural level of the FCD. The Perry River and Frisby Creek localities are 4–5 and 6–7 km structurally below the basement-cover contact, respectively, and each expose ~3 km^2 of continuous outcrops polished by retreating glaciers. At both localities, the Paleoproterozoic, pre-Bourne granite history is complex and its documentation is beyond the scope of this study. Bourne granite dykes are ubiquitous and crosscut recumbent folds and their axial-planar migmatitic gneissosity at a high angle (Fig. 11A and C). A lineation was not observed at Frisby Creek, whereas the E–W lineation observed at some outcrops at Perry River is cut by Bourne granite dyke (Fig. 11D). Consequently, regardless of complexities described below, there is no Cordilleran penetrative ductile fabric within a 6–7 km thick section of basement occurring below the transition zone, which makes the mega-boudin hypothesis unlikely.

6. Localized Cordilleran strain in the lower basement

6.1. Top-to-the-east shear zone at Bourne Glacier

Despite evidence presented above for the absence of penetrative Cordilleran ductile strain at Bourne Glacier, a thin, 10–20 m thick, shear zone in a paragneiss sliver can be confidently attributed to Cordilleran deformation. The zone is characterized by abundant kinematic indicators, such as C–S fabric, shear bands and oblique boudin trains (Hanmer and Passchier, 1991), all indicating a top-to-the-east sense of shear (Fig. 12). Shearing was apparently limited to softer schist, because the surrounding orthogneiss was not affected. The maximum age of shearing is provided by the ~1850 Ma crystallization age of a pegmatite dyke (Crowley et al., 2008) that is trapped and dismembered into oblique boudins in the zone. We estimate that shearing occurred at ~51 Ma from the age of fluid-derived monazites in that same dyke (Crowley et al., 2008), and from monazite that grew in a nearby pelitic schist (Crowley and Parrish, 1999; Crowley and Ghent, 1999).

6.2. Upright folding and partial melting

In the lower basement, local upright folds postdate intrusion of Bourne granite dykes. At Frisby Creek, upright, open, non-cylindrical folds with shallow axes and steep, NNW–SSE axial planes fold the migmatitic gneissosity and Bourne granite dykes (Fig. 11B, C). Granitic leucosome veins containing coarse (>5 mm in diameter) euhedral hornblende and small (<2 mm in diameter) garnet are common (Fig. 11B) and parallel to the NNW–SSE axial planes of the folds. Folding was temporally associated with the leucosome

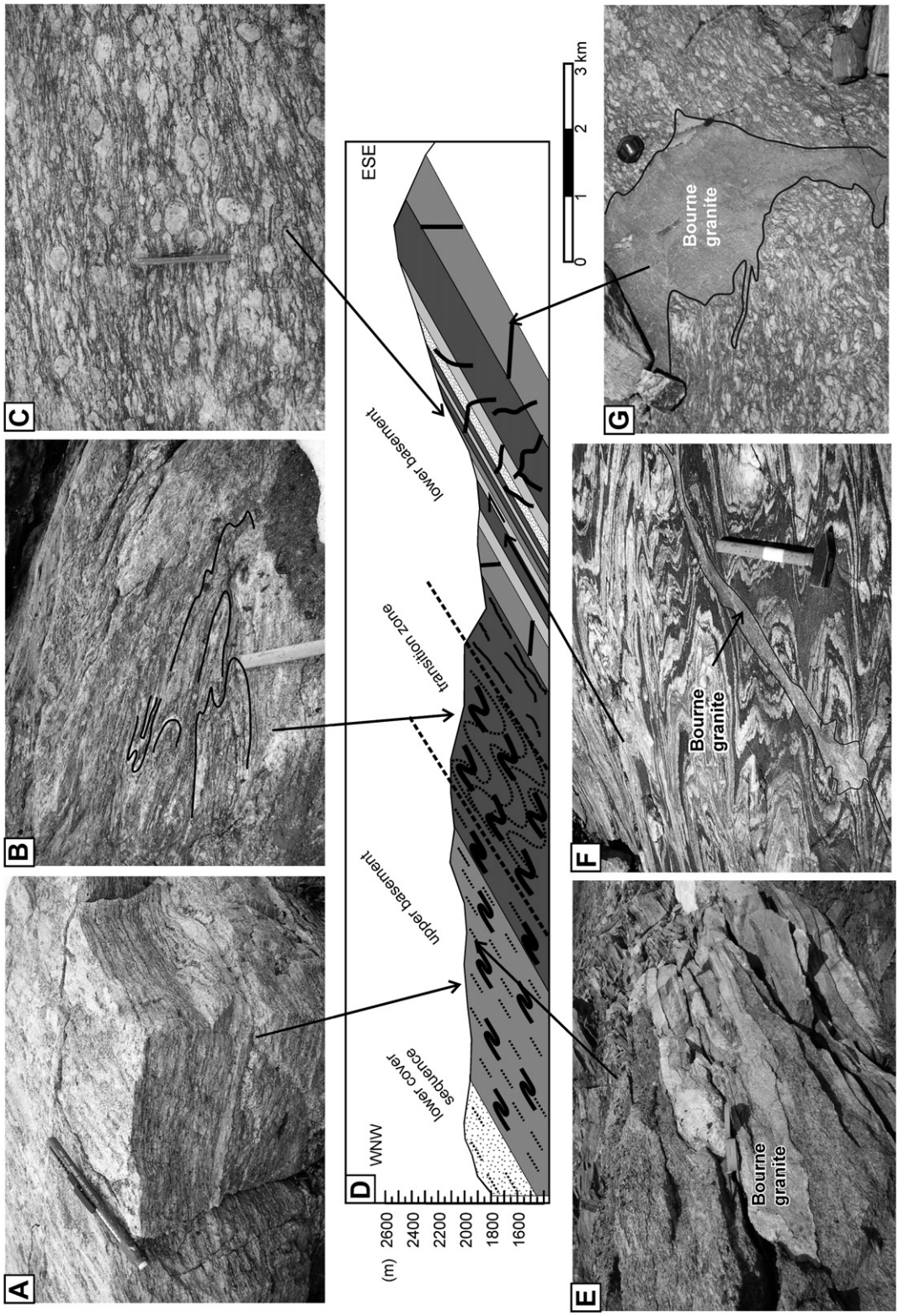

Fig. 9. WNW–ESE geological cross-section and field relationships from the area surrounding the northern toe of Bourne Glacier (location on Fig. 3). (A–C) Strain gradient developed in the ~2.1 Ga granodioritic augen gneiss. The augen gneiss is completely transposed in the upper basement with a strong LS fabric (A), highly folded in the transition zone (B), and primary cores of K-feldspar are still present in augen in the lower basement (C). (D) WNW–ESE cross-section. Same fill patterns as on the map of Fig. 3A, except for thick black lines that illustrate the deformation state of Bourne granite dykes. Vertical scale = horizontal scale. (E) Isoclinal and recumbent fold developed in Bourne granite dyke in the upper basement. (F) Thin Bourne granite dyke crosscuts a fold train in the lower basement. (G) Weakly deformed Bourne granite dyke crosscuts the foliation in granodioritic augen gneiss at a high angle in the lower basement.

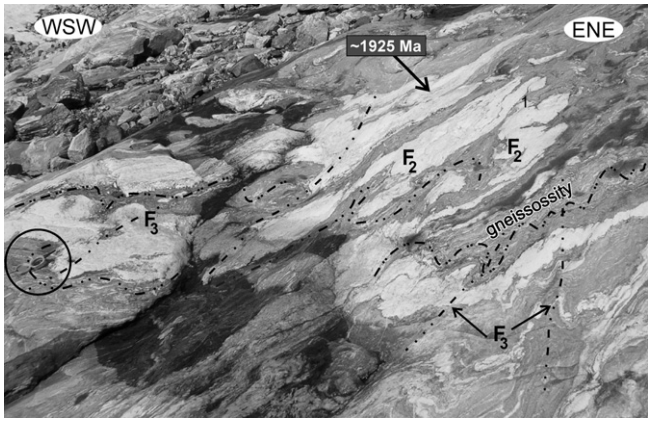

Fig. 10. Pegmatitic layer (leucosome?) sample JC-09-03 from Bourne Glacier locality dated at ~1925 Ma (Crowley et al., 2008). It is folded into an isoclinal F_2 fold that is axial-planar to the gneissosity of the host gneiss and refolded by upright N–S trending F_3 folds. This sample is less than ~100 m away from samples JC-08-03 and JC-308-03, which are ~1850 Ma pegmatite dykes that crosscut the gneissosity at a high angle (Crowley et al., 2008). The age of the migmatitic gneissosity is thus bracketed between 1925 and 1850 Ma. Compass for scale at the left is circled.

veins because the amplitude of folds increases at their margin, and the migmatitic gneissosity is commonly disrupted across it. Deformation is heterogeneously distributed. For example, Fig. 11A depicts a Bourne granite dyke cutting across both limbs of a recumbent fold and its axial-planar migmatitic gneissosity. There, upright folds and hornblende-bearing leucosomes are absent. In contrast, ~10 m to the east, within the same outcrop and the same lithologic units, upright folds and hornblende-bearing leucosome abound, and a Bourne granite dyke (sample FG-425b-05 analysed for its chemical composition; Fig. 5) is oriented parallel to the axial surface of the upright folds (Fig. 11B). Such heterogeneous distribution of upright folds, hornblende-bearing leucosome, and Bourne granite dykes that cut the gneissosity at a high angle is a striking characteristic of both localities. These observations imply that the migmatitic gneissosity is older than the ~1850 Ma Bourne granite, and that the upright folds and associated hornblende-bearing leucosome are younger.

6.2.1. U–Pb geochronology of hornblende-bearing leucosome

Zircon extracted from hornblende-bearing leucosome veins collected at the Perry River and Frisby Creek localities were dated following the analytical method outlined above. All grains except for one have a euhedral and elongate prismatic shape, strong oscillatory zoning from core to rim, and bright CL images (Fig. 14A). Thirty-five dates from thirty grains from two samples (FG-425c-05

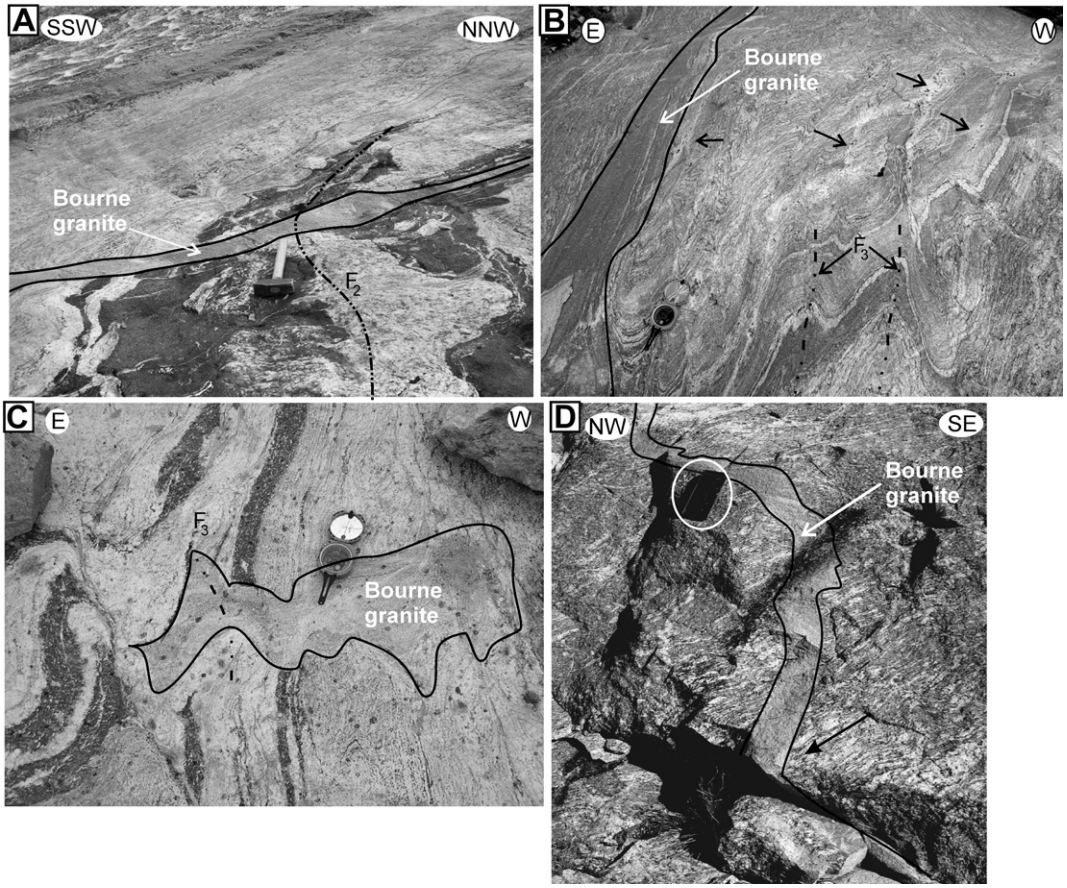

Fig. 11. Field relationships between Bourne granite dykes and host gneisses in the lower basement at Frisby Creek and Perry River localities. (A) Straight and undeformed Bourne granite dyke crosscuts both limbs of an isoclinally folded mafic layer (Frisby Creek locality). Hammer for scale. (B) ~10 m east of (A) the migmatitic gneissosity is folded by open NNW–SSE trending F_3 folds associated with steeply dipping, axial-planar, hornblende + garnet-bearing leucosome veins (unlabeled black arrows). A Bourne granite dyke (contoured on the far left of the photo) is transposed parallel to steep F_3 axial plane. F_3 is thus localized and younger than ~1850 Ma. Compass pointing to N for scale. (C) A Bourne granite dyke crosscuts the gneissic layering at right angle, and was folded by open, NNW–SSE trending F_3 fold (Frisby Creek locality). Compass pointing to N for scale. (D) A Bourne granite dyke crosscuts an E–W stretching lineation (black arrow) developed in the host granodioritic augen gneiss (Perry River locality). Despite the lineation having an orientation typical of Cordilleran lineations, it must be older than the ~1850 Bourne granite dyke. Notebook for scale is circled.

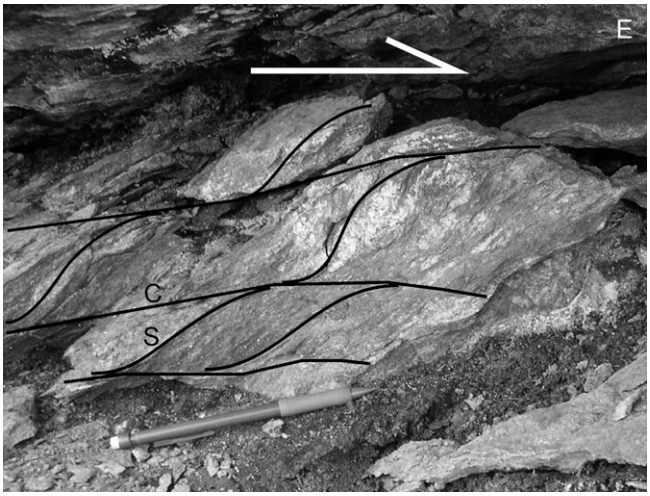

Fig. 12. Meter-scale ductile shear zone with a top-to-the-east sense of shear at the Bourne Glacier locality. C–S fabric developed within a garnet–sillimanite–biotite schist containing leucosome. The leucosome is thought to have been derived from the same material as the ~1850 Ma pegmatite JC-308-03 (Crowley et al., 2008) that is dismembered into an oblique boudin train elsewhere in the same outcrop.

and JC-42-05; Table 4) define a discordia with upper and lower intercepts of 2114 ± 27 and 564 ± 140 Ma, respectively (MSWD = 0.74; prob. = 0.86; Fig. 14C). One grain from sample FG-425c-05 differs from the others by having an inherited core, dark CL image, and faint oscillatory zoning (Fig. 14B). Three analyses from outside the inherited core yielded a weighted mean $^{206}Pb/^{238}U$ date of 52.7 ± 1.1 Ma (MSWD = 0.47; prob. = 0.63; Fig. 14D).

The crystallization age of hornblende-bearing leucosome veins cannot be given by the upper intercept of the discordia defined by thirty-five dates because ~2100 Ma is >300 m y older than the Bourne granite dykes that predate the leucosome and associated upright folds. All grains except one are thus interpreted as being inherited from the host granodioritic orthogneiss that crystallized at ~2100 Ma, whereas the lone Eocene zircon is interpreted as being the product of crystallization of the leucosome. We interpret that the crystallization age of the leucosome and associated folding is provided by the 52.7 ± 1.1 Ma age from one zircon (Fig. 14D). This age is slightly older than the 49.3 ± 1.1 Ma age from titanite from sample JC-50-03 (Fig. 7C), is consistent with the timing of deformation and metamorphic peak in the upper basement (Crowley and Parrish, 1999; Crowley et al., 2001), as well as with our estimate for the timing of shearing at Bourne Glacier (see above).

A portion of the leucosome in the FCD therefore formed synchronously with Early Eocene leucosome in the TOD (Vanderhaeghe et al., 1999; Hinchey et al., 2006). However, in contrast to interpretations of the TOD leucosome (e.g., Vanderhaeghe et al., 1999; Teyssier et al., 2005), we conclude that the FCD leucosome does not reflect extensive melting and extreme ductile flow in Early Eocene because they are localized rather than ubiquitous. Between partially molten and folded zones, Bourne granite dykes are undeformed and cut the migmatitic gneissosity at high angles (Figs. 9F, G and 11A, C, D). Even in reworked zones, gneissic layering is commonly only weakly disrupted (Fig. 11B). Such strain localization is not expected in migmatitic terrains affected by dehydration melting. In these migmatites, melting starts at grain boundaries and the melt phase migrates to dilatant sites with deformation (e.g., Sawyer, 1999; Rosenberg and Berger, 2001; Brown, 2007). Rosenberg and Handy (2005) showed that a significant reduction of strength occurs when melt volume reaches ~7%, at which point the migmatite should flow and develop penetrative ductile fabrics. The result of this behaviour is not observed in the FCD, where deformation is limited to open folds and discrete leucosome veins.

We argue that melting in the FCD was instead induced by and limited to zones of fluid infiltration. Independent evidence for genesis of leucosome via fluid-assisted melting is the abundance of coarse hornblende in leucosome that requires the addition of a significant amount of water (>5 wt%), according to the partial melting experiment of Naney and Swanson (1980), which were conducted on a synthetic Fe–Mg granodioritic sample comparable to the main granodioritic augen gneiss of the FCD. The growth of Eocene monazite with variable chemical composition and zoning in a pegmatite of the Bourne suite (Crowley et al., 2008) is further evidence for Eocene fluid infiltration into the basement.

7. Discussion

7.1. A Cordilleran orogenic base

Our data complement those from Crowley et al. (2001, 2008) to demonstrate that grey granite dykes of the Bourne suite intruded in the basement gneiss of the FCD at ~1850 Ma. The Bourne granite suite is used as a structural-time marker to show that only the upper ~1.5 km of the basement records penetrative Cordilleran strain. Below this carapace of high Cordilleran strain, Bourne granite dykes crosscut a gneissosity throughout the exposed 4–5 km thick lower basement. The boundary between these two structural levels is transitional and characterized by abundant easterly verging folds with few lineations. Waning of Cordilleran strain with structural depth is not related to strain partitioning into softer lithologic units because it occurs within the same orthogneissic units (Fig. 3A). This boundary also coincides with a major change of strain patterns. Above the transition zone, a 17–22 km-thick structural section comprising the Lower Selkirk allochthon, the upper and lower cover sequence and the upper basement, is characterized by a well-developed, W- to SW-plunging stretching lineation, toward which minor fold axes have been almost completely rotated (Fig. 2; Gervais, 2009) during easterly directed shearing. In stark contrast, gneisses in the lower basement have weak lineations that do not cluster on lower-hemisphere, equal-area projections (Fig. 3E) and no kinematic indicators were observed. Therefore, the transition zone likely represents the base of easterly verging shearing in the southeastern Canadian Cordillera. Furthermore, as previously argued (Armstrong et al., 1991; Crowley and Parrish, 1999; Crowley et al., 2001), the lower basement level of the FCD must have been deeply buried only for a few million years because: 1) it lacks penetrative deformation (this study); 2) it lacks evidence for Cordilleran metamorphism and deformation prior to ~53 Ma (Crowley and Parrish, 1999; Crowley and Ghent, 1999; Crowley et al., 2001; this study); and 3) Paleoproterozoic Pb is preserved in titanite (Crowley, 1999; Crowley and Parrish, 1999; this study), which implies a short residence time at high temperature (Cherniak, 1993). This latter evidence implies that gneisses of the lower basement were not underthrust beneath rocks located structurally above the transition zone until the Paleocene, at the earliest, and must have lain further inboard, toward the foreland.

These findings are at odds with the high ductility recorded in the core of the TOD. However, it is likely that the base of Cordilleran deformation occurs in the subsurface of the TOD or in outcrops for which the age of deformation remains to be determined. Our findings indicate that the orogenic base in the FCD occurs approximately 1.5 km structurally below the basal quartzite, but all the studies documenting Eocene high strain and partial melting in the TOD were conducted at less than ~1.5 km from the lowest exposure of cover rocks (Fig. 1; Vanderhaeghe et al., 1999; Johnston

et al., 2000; Norlander et al., 2002; Hinchey et al., 2006). At a structural level of ~2.5 km below the basal quartzite, the Frigg Glacier area is one exception. The structural characteristics of the Frigg Glacier area in the TOD are similar to those of the Frisby Creek locality in the FCD (compare Fig. 13A and B). Moreover, an aplitic dyke dated by Kuiper (2003) has the same relative chronology of field relationships (i.e., crosscuts all structures except the late folds and spatially associated leucosome veins) and similar U–Pb zircon systematics as the Bourne granite (i.e., zircon records ~1.9 and 0.5 Ga growth). Further work is clearly needed to prove whether the core of the TOD also preserves a Paleoproterozoic gneissosity, but the remarkable structural and geochronological similarities between the deepest structural levels of the two domes suggest it may.

7.2. Implication for gneiss dome formation and gravitational collapse models

For the past 25 years, formation of gneiss domes in the southeastern Canadian Cordillera has been linked to post-collisional extension (Coney and Harms, 1984; Carr et al., 1987; Parrish et al., 1988; Vanderhaeghe et al., 1999; Vanderhaeghe and Teyssier, 2001; Norlander et al., 2002; Price and Monger, 2003; Teyssier and Whitney, 2002; Teyssier et al., 2005; Kruse and Williams, 2007). However, several lines of reasoning suggest that extensional models of doming are not applicable to the FCD. First, the presence of NNE-trending upright folds, rather than boudins and lineations, at the deepest-exposed structural level of the FCD is not compatible with E–W extension. Second, extension should have produced Eocene intrusive rocks in the basement, whereas none have been found aside from the ~48 Ma lamprophyre dykes. Third, westerly dipping, easterly verging structures formed by E–W extension can only result from back-rotation of a normal shear zone initially dipping to the east (as in a rolling-hinge c.f. Brun et al., 1994 and Teyssier et al., 2005). This scenario does not apply to the FCD because the intensely deformed easterly verging rocks of the lower cover sequence and upper basement are part of a fold-nappe stack, through which the orientation of foliation and lineation is unchanged (Fig. 2). In addition, the presence of kyanite-K-feldspar metapelitic schist and sillimanite-K-feldspar metapelitic schist in the upper and lower levels of the cover sequence, respectively, is the opposite of the lower-pressure over higher-pressure distribution expected across a normal shear zone. Fourth, a distinctive criterion of models for core complexes is the dissection of the upper crust by normal faulting, which is not observed in hanging wall rocks of the Columbia River fault that bounds the east margin of the Monashee Complex (Crowley and Brown, 1994; Colpron et al., 1996). Last and foremost, models involving ductile flow of rocks coring domes (e.g., Coney and Harms, 1984; Vanderhaeghe et al., 1999; Teyssier et al., 2005; Tirel et al., 2008; Rey et al., 2009), are incompatible with the absence of a Cordilleran foliation in the lower basement of the FCD.

Studies in the TOD were pivotal to deriving the paradigm of post-collisional gravitational collapse inducing lateral and vertical flow of a partially molten middle crust to form gneiss domes (Vanderhaeghe et al., 1999; Rey et al., 2001; Vanderhaeghe and Teyssier, 2001; Teyssier and Whitney, 2002; Whitney et al., 2004; Teyssier et al., 2005). However, the absence of penetrative deformation in the core of the FCD combined with the absence of a crustal-scale shear zone between the domes (NW–SE cross-section in Fig. 1; Read, 1980) rules out the vertical flow model for gneiss domes formation and the free-boundary mode of gravitational collapse (Rey et al., 2001; Teyssier et al., 2005). On the other hand, the fixed-boundary collapse mode of Rey et al. (2001) cannot be ruled out. In this model, collapse of a thick crustal welt induces foreland-directed flow in the middle crust, which results in thrusting and metamorphism in the foreland regions. Applied to the Canadian Cordillera, this model would imply that high-grade rocks above the transition zone (i.e., the Monashee Complex and the Lower Selkirk allochthon) would have been part of a channel that would have flowed up a basement ramp. The test of this model, which requires evaluation of data from a much larger area, will be presented elsewhere, but the data presented herein cannot exclude it.

7.3. Strain pattern distribution at the end of the Cordilleran orogeny and formation of the FCD

We build upon the data from Crowley et al. (2001) to present a more complete picture of the distribution of structures throughout the FCD in the Eocene (Table 5). On the west flank of the dome in the lower cover sequence, part of the transposition foliation formed by easterly verging shear strain after ~50.5 Ma. On the northeast-dipping flank of the dome, in the lower cover sequence and upper basement, part of the transposition foliation and the northeast-verging F_3 folds formed between 52 and 49.5 Ma. On the westerly dipping flank of the dome in the lower basement (Bourne Glacier locality), a top-to-the-east shear zone developed at

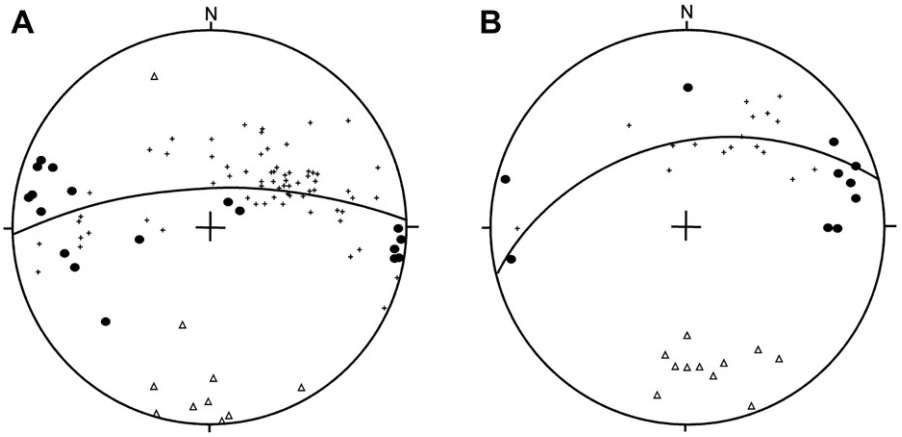

Fig. 13. Equal-area, lower-hemisphere projections showing similarity of structural data from: A) the Frigg Glacier area in the TOD (redrawn from Blattner, 1971); and B) the Frisby Creek locality in the FCD. Crosses: pole to gneissosity; filled circles: poles to leucosome veins; open triangles: fold axes; great circles: best-fit girdle passing through poles to gneissosity.

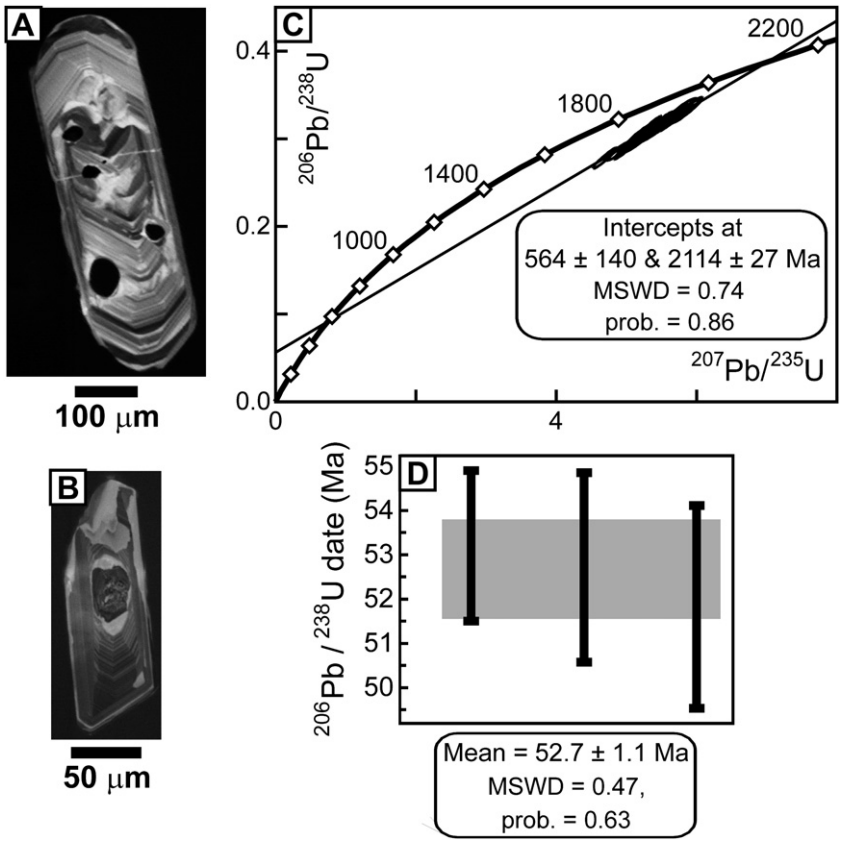

Fig. 14. U–Pb zircon LA-MC-CP-MS geochronology of hornblende-bearing leucosome samples FG-425c-05 and JC-42-05 from the Frisby Creek and Perry River localities, respectively. (A) CL image of a typical oscillatory-zoned zircon inherited from the host granodioritic augen gneiss. (B) CL image of the only Eocene zircon extracted from the hornblende-bearing leucosome. (C) Concordia plot of 35 analyses from 30 inherited zircon grains from the two samples. The upper intercept of 2114 ± 27 Ma is interpreted as the crystallization age of the host granodioritic augen gneiss. Ellipses plotted at 2σ. (D) Plot of $^{206}Pb/^{238}U$ dates from the lone Eocene zircon extracted from the two leucosomes (error is 2σ). The weighted mean $^{206}Pb/^{238}U$ date of 52.7 ± 1.1 Ma is interpreted as the crystallization age. Both plots made with Isoplot3 (Ludwig, 2008). MSWD = Mean Square of Weighted Deviates. prob. = probability of fit.

~51 Ma. Finally, on the southerly dipping, deepest-exposed structural level of the FCD, NNE-trending upright folds formed at ~53 Ma. All structures surrounding the FCD thus formed between 53 and 49 Ma, which coincides with or shortly predates regional cooling in the southern Omineca Belt.

Inasmuch as each flank of the FCD is characterized by specific structures, their development must be coeval with the formation of the dome. Therefore, the well-constrained timing of NE-verging folding on the eastern flank of the dome (Table 5; Crowley et al., 2001) indicates that the FCD formed between 51 and 49 Ma. During this period, there was easterly verging deformation on both the westerly and easterly dipping flanks of the dome while NNE-trending upright folds had just formed, or were forming, in its core. Journeay (1986) argued that buckling, or diapirism and crustal boudinage are not viable doming models because they should result in structures verging toward and away from the dome crest, respectively. A model of arching by three successive stages of piggyback thrusting above basement ramps during easterly verging shearing was instead proposed (see also Brown and Journeay, 1987). However, the evidence of late basement underthrusting presented herein limits the number of possible stages of thrusting above a basement ramp to one. Furthermore, thrusting above a ramp alone would not result in doming of the basement. Some form of basement folding is required. Analogue modeling (Williams et al., 2006) argued that drag folds initially develop as upright folds before being overturned into their typical asymmetric isoclinal geometry (Fig. 15D). We therefore suggest that doming represents the initial stage of a drag fold developed during crustal-scale easterly verging shearing. Thrusting above the basement ramp placed the base of the thrust sheet parallel to the shear plane, thus allowing it to fold. As the dome formed, its easterly dipping flank and now flat-lying core were put in the contractional field of the strain ellipsoid and were folded, while the westerly dipping flank remained in the extensional field and was deformed by layer-parallel shearing, flattening and boudinage (Fig. 15B). Finally, it is interesting to note that Eocene contractional doming models were recently proposed for the TOD (the suprastructure-type folding model of Parmenter and Williams, 2009), and for the Valhalla Complex (basement duplexing model of Carr and Simony, 2006).

Table 5
Summary of Eocene deformation in the FCD.

Structural level	Regional dip of foliation	Structure	Age (Ma)
Lover cover sequence	WSW	top-to-the-E	<50.5[a]
Lover cover sequence	NE	Part of foliation NE-verging F_3	<51[a]
Upper basement	NE	Part of foliation NE-verging F_3	52–49.5[a]
Lower basement (Bourne Glacier)	WSW	meter-scale top-to-the-E shear zone	~51[b]
Lower basement (Frisby Creek)	SSW	upright NNE-trending folds	~53[b]

[a] Crowley et al. (2001).
[b] This study.

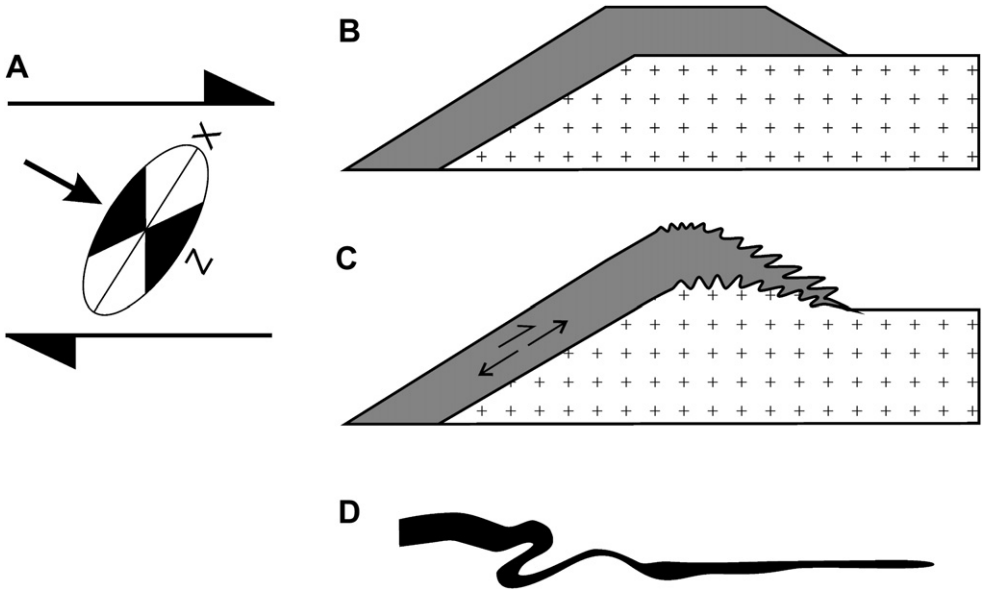

Fig. 15. Kinematic model for the formation of the FCD. A) Orientation of the strain ellipse during crustal-scale easterly verging shearing. B) Underthrusting of a basement ramp reoriented rocks at the base of the thrust sheet into the contractional field of the strain ellipse, which C) led to the formation of a dome by upright folding. In such structural setting, the west flank of the dome records flattening, boudinage and layer-parallel shearing, whereas the core and eastern flank develop upright and easterly verging folds, respectively. D) Development of a drag fold by deformation of analogue material in simple shear (redrawn from Williams et al., 2006; Bons, 1993). The upright fold on the right is a structure formed late in the experiment, and is thus representative of the initial geometry of a drag fold, whereas the easterly verging asymmetric fold to the left is an early-formed structure, and is thus representative of the final geometry. See text for additional details.

This study provides insight into crustal-scale transposition processes. In the Paleocene-Early Eocene, the underthrusting of a basement ramp led to upright folding and the formation of the FCD. A modification of far-field stresses at ~50 Ma induced extension that led to regional cooling and to the formation of major normal faults, such as the Okanagan Valley Fault system to the west (Johnson, 2006) and the Columbia River fault on the east flank of the FCD (Read and Brown, 1983; Mulch et al., 2006). Given that E–W contraction in the upper and lower basement immediately preceded rapid regional cooling and extension that marked the end of orogeny in the southeastern Canadian Cordillera, the deformation patterns provide a snapshot of a downward-migrating base of easterly verging shearing frozen at the end of orogeny. Accordingly, the upper basement represents the lowermost transposed structural level, the transition zone represents a less advanced stage of transposition, and the lower basement represents initial stages of deformation with localized deformation zones characterized by upright folds and thrust shear zones. If contractional deformation had continued, gneisses of the lower basement would most likely have been completely transposed and become similar to gneisses of the upper basement level.

8. Conclusions

1. Similarities in field relationships (Fig. 4A, B), macro- and microscopic textures (Fig. 4C), trace element profiles (Fig. 5) and U–Pb ages (Figs. 6 and 8) demonstrate that grey granite bodies in the basement of the Frenchman Cap dome are related and were intruded at 1.85 Ga. These intrusions, grouped into the Bourne granite suite, are ideal time markers for distinguishing Cordilleran from Paleoproterozoic deformation.
2. A transition zone of decreasing, NE-directed shear strain, marked by abundant folds (Fig. 9B), occurs ~1.5 km below the cover-basement contact in the Frenchman Cap dome (Fig. 9D). Above this zone, and throughout the Monashee Complex and overlying Lower Selkirk allochthon, strain is high and indicates NE-directed shearing (Fig. 2). In contrast, below this transition zone, within a 6–7 km thick structural section, penetrative ductile Cordilleran strain is absent (Fig. 9F and G).
3. Cordilleran strain in the lower basement of the Frenchman Cap dome is limited to (i) a meter-scale, top-to-the-E shear zone located within schistose slivers interlayered with basement orthogneiss at the Bourne Glacier locality (Fig. 12) and (ii) upright NNW–SSE trending folds associated with hornblende-bearing leucosome at the Frisby Creek and Perry River localities (Fig. 11B and C). U–Pb dating indicates that these structures developed at 53–49 Ma.
4. The deformation pattern of flattening, boudinage and easterly verging layer-parallel shear strain on the westerly dipping flank of the dome contrasts with easterly verging upright folding in the dome core and northeast verging folding on the easterly dipping flank of the dome. This study complements previous work by demonstrating that these structures formed synchronously between 53 and 49 Ma, immediately prior to regional cooling and extension.
5. A model of doming by incipient drag folding following thrusting above a basement ramp best fits these structures. No data were found that support an extensional origin for the dome.
6. Our results rule out the widely accepted views that gneiss domes of the southeastern Canadian Cordillera are extensional core complexes (Coney and Harms, 1984; Carr et al., 1987; Parrish et al., 1988; Vanderhaeghe et al., 1999; Vanderhaeghe and Teyssier, 2001; Norlander et al., 2002; Price and Monger, 2003; Teyssier and Whitney, 2002; Teyssier et al., 2005; Kruse and Williams, 2007), and that gneiss domes in general originate from vertical ductile flow (Teyssier and Whitney, 2002; Whitney et al., 2004; Teyssier et al., 2005).
7. Although we cannot exclude a model of thrusting driven by channel flow in a fixed-boundary gravitational collapse mode (Rey et al., 2001), we argue that the above characteristics are

consistent with a frozen, downward-migrating base of convergent shearing. In any case, it implies that the orogenic base of the southern Canadian Cordillera is exposed in the core of the Frenchman Cap dome.

Acknowledgements

This work is part of a PHD thesis conducted by FG under the supervision of RLB. The project was financed by a NSERC Discovery grant held by RLB. A. Simonetti of the Radiogenic Isotopic Facility of University of Alberta is thanked for his assistance during the acquisition of U–Pb LA-MC-ICP-MS data. We are grateful to S. Bowring from the Massachusetts Institute of Technology for providing access to his mineral separation laboratory. D. Vachon and N. Williams are thanked for excellent field assistance. Numerous drafts of this manuscript were carefully edited and considerably improved by S. Carr and J. Percival. Reviews by R. Hatcher and P. Karabinos and editorial handling by W. Dunne significantly improved the quality of the manuscript.

References

Adams, M.G., Lentz, D.R., Shaw, C.S.J., Williams, P.F., Archibald, D.A., Cousens, B., 2005. Eocene shoshonitic mafic dykes intruding the Monashee complex, British Columbia: a petrogenetic relationship with the Kamloops Group volcanic sequence? Canadian Journal of Earth Sciences 42, 11–24.

Aleinikoff, J.N., Horton Jr., J.W., Drake Jr., A.A., Wintsch, R.P., Fanning, C.M., Yi, K., Tollo, R.P., Corriveau, L., McLelland, J., Bartholomew, M.J., 2004. Deciphering multiple Mesoproterozoic and Paleozoic events recorded in zircon and titanite from the Baltimore Gneiss, Maryland; SEM imaging, SHRIMP U–Pb geochronology, and EMP analysis. Memoir – Geological Society of America 197, 411–434.

Aleinikoff, J.N., Wintsch, R.P., Tollo, R.P., Unruh, D.M., Fanning, C.M., Schmitz, M.D., 2007. Ages and origins of rocks of the Killingworth dome, south-central Connecticut; implications for the tectonic evolution of southern New England. American Journal of Science 307, 63–118.

Armstrong, R.L., Parrish, R.R., van der Heyden, P., Scott, K., Runkle, D., Brown, R.L., Ross, G.M., 1991. Early Proterozoic basement exposures in the southern Canadian Cordillera; core gneiss of Frenchman Cap, unit I of the Grand Forks gneiss, and the Vaseaux formation. Canadian Journal of Earth Sciences 28, 1169–1201.

Bardoux M., 1994. The Okanagan Valley Normal Fault from Penticton to Enderby, South-central British Columbia. Doctoral thesis, Carleton University, 292 pp.

Beard, J.S., Sorensen, S.S., Gieré, R., 2006. REE zoning in allanite related to changing partition coefficients during crystallization: Implications for REE behaviour in an epidote-bearing tonalite. Mineralogical Magazine 70, 419–435.

Blattner, P., 1971. Migmatite by partial fusion and short-range hydrothermal transfer, British Columbia. Schweizerische Mineralogische und Petrographische Mitteilungen 51, 155–177.

Björnson L.T., 2003. Structure of the Mount Copeland area, Monashee Complex, Southeastern British Columbia. Master's thesis, Carleton University, 149 pp.

Bons, P.D., 1993. Experimental deformation of polyphase rock analogues. Geologica Ultrajectina: Mededelingen van de Faculteit Aardwetenschappen der Universiteit Utrecht 110, 1–207.

Brown, M., 2007. Crustal melting and melt extraction, ascent and emplacement in orogens; mechanisms and consequences. Journal of the Geological Society of London 164, 709–730.

Brown, R.L., 2004. Thrust-belt accretion and hinterland underplating of orogenic wedges; an example from the Canadian Cordillera. AAPG Memoir 82, 51–64.

Brown, R.L., Journeay, M.J., 1987. Tectonic denudation of the Shuswap metamorphic terrane of southeastern British Columbia. Geology 15, 142–146.

Brown, R.L., Psutka, J.F., 1980. Structural and stratigraphic setting of the Downie Slide, Columbia River valley, British Columbia. Canadian Journal of Earth Sciences 17, 698–709.

Brun, J.P., Sokoutis, D., Van Den Driessche, J., 1994. Analogue modeling of detachment fault systems and core complexes. Geology 22, 319–322.

Carr, S.D., Parrish, R.R., Brown, R.L., 1987. Eocene structural development of the Valhalla complex, southeastern British Columbia. Tectonics 6, 175–196.

Carr, S.D., Simony, P.S., 2006. Ductile thrusting versus channel flow in the southeastern Canadian Cordillera; evolution of a coherent crystalline thrust sheet. In: Law, R.D., Searle, M.P., Godin, L. (Eds.), Channel Flow, Ductile Extrusion and Exhumation in Continental Collision Zones. Geological Society, London, Special Publication, vol. 268, pp. 561–587.

Cherniak, D.J., 1993. Lead diffusion in titanite and preliminary results on the effects of radiation damage on Pb transport. Chemical Geology 110, 177–194.

Colpron, M., Price, R.A., Archibald, D.A., Carmichael, D.M., 1996. Middle Jurassic exhumation along the western flank of the Selkirk fan structure; thermobarometric and thermochronometric constraints from the Illecillewaet Synclinorium, southeastern British Columbia. Geological Society of America Bulletin 108.

Coney, P.J., Harms, T.A., 1984. Cordilleran metamorphic core complexes; Cenozoic extensional relics of Mesozoic compression. Geology 12, 550–554.

Crowley, J.L., 1999. U–Pb geochronological constraints on Paleoproterozoic tectonism in the Monashee complex, Canadian Cordillera: elucidating an overprinted geologic history. Geological Society of America Bulletin 111, 560–577.

Crowley, J.L., Brown, R.L., 1994. Tectonic links between the Clachnacudainn terrane and Selkirk allochthon, southern Omineca belt, Canadian Cordillera. Tectonics 13, 1035–1051.

Crowley, J.L., Ghent, E.D., 1999. An electron microprobe study of the U–Th–Pb systematics of metamorphosed monazite; the role of Pb diffusion versus overgrowth and recrystallization. Chemical Geology 157, 285–302.

Crowley, J.L., Parrish, R.R., 1999. U–Pb isotopic constraints on diachronous metamorphism in the northern Monashee complex, southern Canadian Cordillera. Journal of Metamorphic Geology 17, 483–502.

Crowley, J.L., Brown, R.L., Parrish, R.R., 2001. Diachronous deformation and a strain gradient beneath the Selkirk allochthon, northern Monashee complex, southeastern Canadian Cordillera. Journal of Structural Geology 23, 1103–1121.

Crowley, J.L., Brown, R.L., Gervais, F., Gibson, H.D., 2008. Assessing inheritance of zircon and monazite in granitic rocks: an example from the Monashee Complex, Canadian Cordillera. Journal of Petrology 49, 1915–1929.

Cuney, M., Friedrich, M., 1987. Physicochemical and crystal-chemical controls on accessory mineral paragenesis in granitoids: implications for uranium metallogenesis. Bulletin de Mineralogie 110, 235–247.

Dini, A., Rocchi, S., Westerman, D.S., 2004. Reaction microtextures of REE-Y-Th-U accessory minerals in the Monte Capanne pluton (Elba Island, Italy): a possible indicator of hybridization processes. Lithos 78, 101–118.

Evenchick, C.A., McMechan, M.E., McNicoll, V.J., Carr, S.D., 2007. A synthesis of the Jurassic–Cretaceous tectonic evolution of the central and southeastern Canadian Cordillera: exploring links across the Orogen. In: Sears, J.W., Harms, T.A., Evenchick, C.A. (Eds.), Whence the Mountains? Inquiries into the Evolution of Orogenic Systems: a Volume in Honor of Raymond A. Price, pp. 117–145.

Foster, G., Parrish, R.R., Horstwood, M.S.A., Chenery, S., Pyle, J., Gibson, H.D., 2004. The generation of prograde P–T–t points and paths; a textural, compositional, and chronological study of metamorphic monazite. Earth and Planetary Science Letters 228, 125–142.

Fyles, J.T., 1970. Structure of the Shuswap metamorphic complex in the Jordan River area, northwest of Revelstoke, British Columbia; structure of the southern Canadian Cordillera. Special Paper - Geological Association of Canada 6, 87–98.

Gervais, F. 2009. Pressure–temperature–time-deformation paths of former mid-crustal rocks, northern Monashee Complex of the southeastern Canadian Cordillera; A model of synconvergent exhumation by sequential ductile extrusion. Doctoral thesis, Carleton University, 325 pp.

Ghent, E., Villeneuve, M., 2006. $^{40}Ar/^{39}Ar$ dates on hornblende, muscovite, and biotite from the Mica Creek area, British Columbia; regional metamorphic and tectonic implications. Canadian Journal of Earth Sciences 43, 83–100.

Gibson, H.D., Brown, R.L., Parrish, R.R., 1999. Deformation-induced inverted metamorphic field gradients: an example from the southeastern Canadian Cordillera. Journal of Structural Geology 21, 751–767.

Glombick, P., Thompson, R.I., Erdmer, P., Daughtry, K.L., 2006. A reappraisal of the tectonic significance of early Tertiary low-angle shear zones exposed in the Vernon map area (82 L), Shuswap metamorphic complex, southeastern Canadian Cordillera. Canadian Journal of Earth Sciences 43, 245–268.

Hanmer, S., Passchier, C., 1991. Shear-sense indicators; a review. Paper – Geological Survey of Canada 90–17, 72.

Hinchey, A.M., Carr, S.D., McNeill, P.D., Rayner, N., 2006. Paleocene–Eocene high-grade metamorphism, anatexis, and deformation in the Thor-Odin dome, Monashee Complex, southeastern British Columbia. Canadian Journal of Earth Sciences 43, 1341–1365.

Hinchey, A.M., Carr, S.D., Rayner, N., 2007. Bulk compositional controls on the preservation of age domains within metamorphic monazite: a case study from quartzite and garnet–cordierite–gedrite gneiss of Thor-Odin dome, Monashee complex, Canadian Cordillera. Chemical Geology 240, 85–102.

Höy, T., Brown, R.L., 1980. Geology of the Eastern Margin of Frenchman Cap Dome. In: British Columbia Ministry of Energy, Mines and Petroleum Resources Bulletin, Preliminary Map No. 43.

Höy, T., 1987. Geology of the Cottonbelt lead–zinc–magnetite layer, carbonatites and alkalic rocks in the Mount Grace area, Frenchman Cap Dome, southeastern British Columbia. Bulletin – Ministry of Energy, Mines and Petroleum Resources 80, 99.

Johnson B.J., 1994. Structure and Tectonic Setting of the Okanagan Valley Fault System in the Shuswap Lake Area, Southern British Columbia. Doctoral thesis, Carleton University, 266 pp.

Johnson, B.J., 2006. Extensional shear zones, granitic melts, and linkage of overstepping normal faults bounding the Shuswap metamorphic core complex, British Columbia. Geological Society of America Bulletin 118, 366–382.

Johnston, D.H., Williams, P.F., Brown, R.L., Crowley, J.L., Carr, S.D., 2000. Northeastward extrusion and extensional exhumation of crystalline rocks of the Monashee Complex, southeastern Canadian Cordillera. Journal of Structural Geology 22, 603–625.

Journeay J.M., 1986. Stratigraphy, Internal Strain and Thermo-tectonic Evolution of Northern Frenchman Cap Dome; an Exhumed Duplex Structure, Omineca Hinterland, S.E. Canadian Cordillera. Doctoral thesis, Queen's University, 421 pp.

Kruse, S., Williams, P.F., 2007. The Monashee reflection; re-examination of a Lithoprobe crustal-scale seismic reflection in the southern Canadian Cordillera. Geosphere 3, 26–41.
Kuiper Y.D., 2003. Isotopic Constraints on Timing of Deformation and Metamorphism in the Thor-Odin Dome, Monashee Complex, Southeastern British Columbia. Doctoral thesis, University of New Brunswick, 290 pp.
Kuiper, Y.D., Williams, P.F., Kruse, S., 2006. Possibility of channel flow in the southern Canadian Cordillera; a new approach to explain existing data. In: Law, R.D., Searle, M.P., Godin, L. (Eds.), Channel Flow, Ductile Extrusion and Exhumation in Continental Collision Zones. Geological Society, London, Special Publication, vol. 268, pp. 589–611.
Lane, L.S., Ghent, E.D., Stout, M.Z., Brown, R.L., 1989. P–T history and kinematics of the Monashee Decollement near Revelstoke, British Columbia. Canadian Journal of Earth Sciences 26, 231–243.
Ludwig, K.R., 2008. User's Manual for Isoplot 3.6. A Geochronological Toolkit for Microsoft Excel. In: Berkeley Geochronological Center, Special Publication, vol. 4, 78 pp.
McMillan, W.J., 1970. West flank, Frenchman's cap gneiss dome, Shuswap terrane, British Columbia; structure of the southern Canadian Cordillera. Special Paper – Geological Association of Canada 6, 99–106.
Mulch, A., Teyssier, C., Cosca, M.A., Vennemann, T.W., 2006. Thermomechanical analysis of strain localization in a ductile detachment zone. Journal of Geophysical Research 111, B12405.
Naney, M.T., Swanson, S.E., 1980. The effect of Fe and Mg on crystallization in granitic systems. American Mineralogist 65, 639–653.
Norlander, B.H., Whitney, D.L., Teyssier, C., Vanderhaeghe, O., 2002. Partial melting and decompression of the Thor-Odin dome, Shuswap metamorphic core complex, Canadian Cordillera. Lithos 61, 103–125.
Passchier, C.W., Myers, J.S., Kröner, A., 1990. Field Geology of High-grade Gneiss Terrains. Springer-Verlag, Berlin.
Parmenter, A.C., Williams, P.F., 2009. Late Superstructure-style Folding of the Monashee Complex Infrastructure. Abstract. In: Geological Association of Canada, 2009 Joint Assembly, vol. 34 GAC23C-02.
Parrish, R.R., 1995. Thermal evolution of the southeastern Canadian Cordillera; the southern Canadian Cordillera Transect of Lithoprobe. Canadian Journal of Earth Sciences 32, 1618–1642.
Parrish, R.R., Carr, S.D., Parkinson, D.L., 1988. Eocene extensional tectonics and geochronology of the southern Omineca belt, British Columbia and Washington. Tectonics 7, 181–212.
Price, R.A., Sears, J.W., 2000. A preliminary palinspastic map of the Mesoproterozoic belt-Purcell Supergroup, Canada and USA; implications for the tectonic setting and structural evolution of the Purcell Anticlinorium and the Sullivan Deposit. In: Lydon, J.W., Höy, T., Slack, J.F., Knapp, M. (Eds.), The Geological Environment of the Sullivan Deposit, British Columbia. Geological Association of Canada, Mineral Deposits Division, Special Publication, 1, pp. 61–81.
Price, R.A., Monger, J.W.H., 2003. A Transect of the Southern Canadian Cordillera from Calgary to Vancouver, May 2003. Geological Association of Canada, Cordilleran Section, Vancouver, 167 pp.
Read, P.B., 1980. Stratigraphy and structure; Thor-Odin to Frenchman Cap "domes", Vernon east-half map area, southern British Columbia. Current research, part A. Paper – Geological Survey of Canada, 19–25.
Reesor, J.E., Moore Jr., J.M., 1971. Petrology and structure of Thor-Odin gneiss dome, Shuswap metamorphic complex, British Columbia. Bulletin – Geological Survey of Canada 195, 149.
Rey, P.F., Vanderhaeghe, O., Teyssier, C., 2001. Gravitational collapse of the continental crust: definition, regimes and modes. Tectonophysics 342, 435–449.
Rey, P.F., Teyssier, C., Whitney, D.L., 2009. Extension rates, crustal melting, and core complex dynamics. Geology 37, 391–394.
Rosenberg, C.L., Berger, A., 2001. Syntectonic melt pathways in granitic gneisses, and melt-induced transitions in deformation mechanisms. Physics and Chemistry of the Earth Part A: Solid Earth and Geodesy 26, 287–293.
Rosenberg, C.L., Handy, M.R., 2005. Experimental deformation of partially melted granite revisited: implications for the continental crust. Journal of Metamorphic Geology 23, 19–28.
Sanborn, N., 1996. Constraints on the Timing and Conditions of Cordilleran Tectonism in Frenchman Cap Dome, Monashee Complex, Southeastern British Columbia from $^{40}Ar/^{39}Ar$ Geochronology. Honours thesis, Queen's University, 40 pp.
Sawyer, E.W., 1999. Criteria for the recognition of partial melting. Physics and Chemistry of the Earth, Part A: Solid Earth and Geodesy 24, 269–279.
Scammell R.J., 1986. Stratigraphy, Structure and Metamorphism of the North Flank of the Monashee Complex, Southeastern British-Columbia: A Record of Proterozoic Extension and Phanerozoic Crustal Thickening. Master thesis, Carleton University, 205 pp.
Scammell R.J., 1993. Mid-Cretaceous to Tertiary Thermotectonic History of Former Mid-crustal Rocks, Southern Omineca Belt, Canadian Cordillera. Doctoral thesis, Queen's University, 576 pp.
Scammell, R.J., Brown, R.L., 1990. Cover gneisses of the Monashee terrane; a record of synsedimentary rifting in the North American Cordillera. Canadian Journal of Earth Sciences 27, 712–726.
Simonetti, A., Heaman, L.M., Hartlaub, R.P., Creaser, R.A., Machattie, T.G., Böhm, C., 2005. U–Pb zircon dating by laser ablation-MC-ICP-MS using a new multiple ion counting faraday collector array. Journal of Analytical Atomic Spectrometry 20, 677–686.
Simonetti, A., Heaman, L.M., Chacko, T., Banerjee, N.R., 2006. In situ petrographic thin section U–Pb dating of zircon, monazite, and titanite using laser ablation-MC-ICP-MS. International Journal of Mass Spectrometry 253, 87–97.
Stacey, J.S., Kramers, J.D., 1975. Approximation of terrestrial lead isotope evolution by a two-stage model. Earth and Planetary Science Letters 26, 207–221.
Storey, C.D., Jeffries, T.E., Smith, M., 2006. Common lead-corrected laser ablation ICP-MS U/Pb systematics and geochronology of titanite. Chemical Geology 227, 37–52.
Teyssier, C., Whitney, D.L., 2002. Gneiss domes and orogeny. Geology 30, 1139–1142.
Teyssier, C., Whitney, D.L., Norlander, B., Ferré, E.C., Vanderhaeghe, O., Parkinson, D., 2005. Flow of partially molten crust and origin of detachments during collapse of the Cordilleran Orogen. In: Bruhn, D., Burlini, L. (Eds.), High-strain Zones: Structure and Physical Properties. Geological Society, London, Special Publication, vol. 245, pp. 39–64.
Tirel, C., Brun, J.P., Burov, E., 2008. Dynamics and structural development of metamorphic core complexes. Journal of Geophysical Research 113, B04403.
Vanderhaeghe, O., Teyssier, C., 2001. Crustal-scale rheological transitions during late-orogenic collapse. Tectonophysics 335, 211–228.
Vanderhaeghe, O., Teyssier, C., Wysoczanski, R., 1999. Structural and geochronological constraints on the role of partial melting during the formation of the Shuswap metamorphic core complex at the latitude of the Thor-Odin Dome, British Columbia. Canadian Journal of Earth Sciences 36, 917–943.
Vanderhaeghe, O., Teyssier, C., McDougall, I., Dunlap, W.J., 2003. Cooling and exhumation of the Shuswap metamorphic core complex constrained by $^{40}Ar/^{39}Ar$ thermochronology. Geological Society of America Bulletin 115, 200–216.
Wheeler, J.O., 1965. Big Bend Map-area, British Columbia, 82M (East Half). Paper. Geological Survey of Canada, 37 pp.
Wheeler, J.O., Brookfield, A.J., Gabrielse, H., Monger, J.W.H., Tipper, H.W., Woodsworth, G.J., 1991. Terrane Map of the Canadian Cordillera, Map 1713A, Scale1:2 000 000. Geological Survey of Canada, Ottawa.
Whitney, D.L., Teyssier, C., Vanderhaeghe, O., 2004. Gneiss domes and crustal flow. In: Whitney, D.L., Teyssier, C., Siddoway, C.S. (Eds.), Gneiss Domes in Orogeny. Special Paper – Geological Society of America, vol. 380, pp. 15–33.
Williams, M.L., Karlstrom, K.E., Dumond, G., Mahan, K.H., 2009. Perspectives on the architecture of continental crust from integrated feld studies of exposed isobaric sections. In: Miller, R.B., Snoke, A.W. (Eds.), Crustal Cross Sections from the Western North American Cordillera and Elsewhere: Implications for Tectonic and Petrologic Processes. Special Paper – Geological Society of America, vol. 456, pp. 219–241.
Williams, P.F., 1985. Multiply deformed terrains-problems of correlation. Journal of Structural Geology 7, 269–280.
Williams, P.F., Jiang, D., 2005. An investigation of lower crustal deformation; evidence for channel flow and its implications for tectonics and structural studies. Journal of Structural Geology 27, 1486–1504.
Williams, P.F., Jiang, D., Lin, S., 2006. Interpretation of deformation fabrics of infrastructure zone rocks in the context of channel flow and other tectonic models. In: Law, R.D., Searle, M.P., Godin, L. (Eds.), Channel Flow, Ductile Extrusion and Exhumation in Continental Collision Zones. Geological Society, London, Special Publication, vol. 268, pp. 221–235.